

In presenting this thesis in partial fulfillment of the requirements for an advanced degree at Idaho State University, I agree that the Library shall make it freely available for inspection. I further state that permission to download and/or print my thesis for scholarly purposes may be granted by the Dean of the Graduate School, Dean of my academic division, or by the University Librarian. It is understood that any copying or publication of this thesis for financial gain shall not be allowed without my written permission.

Signature _____

Date _____

APPLICATIONS OF ADVANCED REMOTE SENSING TECHNIQUES
FOR CHARACTERIZING FOREST TERRAIN

by

Matthew E. Belt

A thesis

submitted in partial fulfillment

of the requirements for the degree of

Master of Science in the Department of Geosciences

Idaho State University

May 2015

Committee Approval

To the Graduate Faculty:

The members of the committee appointed to examine the thesis of Matthew Belt find it satisfactory and recommend that it be accepted.

Dr. Donna Delparte,
Major Advisor

Dr. Nancy Glenn,
Committee Member

Dr. Yolonda Youngs,
Graduate Faculty Representative

TABLE OF CONTENTS

LIST OF FIGURES	VI
LIST OF TABLES	VIII
THESIS ABSTRACT	IX
CHAPTER 1. INTRODUCTION AND BACKGROUND	1
STATEMENT OF PURPOSE	1
TERRETRIAL LASER SCANNING	5
MULTISPRECTRAL IMAGERY	7
DATA FUSION	9
CHAPTER 2. SPATIAL MODELING OF DENSLY VEGETATED TERRAIN WITH GEOMETRIC FILTERING TECHNIQUES USING TERESTRIAL LASER SCANNING (TLS)	10
INTRODUCTION	10
METHODS	13
<i>Data Collection</i>	14
<i>Data Pre-Processing</i>	15
<i>Terrain Processing and Normalization</i>	18
<i>Canopy Height Model Processing and Normalization</i>	21
RESULTS	23
<i>Empirical error estimates</i>	24
DISCUSSION	24
<i>Sources of Error</i>	26
<i>Comparative Alternatives</i>	28
ACKNOWLEDGMENTS	29
LITERATURE CITED	30

CHAPTER 3. FOREST CLASSIFICATION USING TERRESTRIAL LIDAR ENHANCED WORLDVIEW-2

MULTISPECTRAL IMAGERY 43

INTRODUCTION 43

METHODS 46

Study Site 46

Data Collection 48

Imagery and LiDAR Co-Registration 50

Image Segmentation 51

Image Classification 52

Prediction Modeling 53

RESULTS 53

Classification Attributes 53

Cover type classification 54

Classification Confidence 55

DISCUSSION 56

Image Segmentation 56

Training and Classification 56

ACKNOWLEDGMENTS 58

LITERATURE CITED 59

CHAPTER 4. CONCLUSION 73

LITERATURE CITED 77

LIST OF FIGURES

CHAPTER 2.

FIGURE 1: Scan locations at the Kauhakō crater study site. GPS positions were collected using a Trimble GeoXH 6000. Contours produced from resulting DTM product with 5 m spacing.	34
FIGURE 2: Classification workflow for TLS point cloud processing and derivative products.	35
FIGURE 3: Sparse point cloud consisting of roughly 49 million points. Duplicate points have been removed with an average sample spacing of 10 cm. Color scale is indicative of surface reflectance. Healthy vegetation is distinctly less reflective than bare earth.	36
FIGURE 4: Height grid filter 1m (C_2). Result of noise removal using curvature, roughness, and nearest neighbor statistics (C_6). Final DTM result: Post SOR filtering, Delaunay mesh resampled to 100 pts/m (C_9).	37
FIGURE 5: Coverage map showing areas defined as non-noise vs. areas that were classified as noise, cleaned then interpolated using Delaunay triangulation.	38
FIGURE 6: <i>Rasterized DTM produced from (C_9). The resulting product has a 50 cm GSD with 5 m minor contour lines and 25 m major contour.</i>	39
FIGURE 7: Comparison between estimated elevation values. TLS derived feature elevations (Top). Estimated elevation values for filtered ground surface (Middle). Normalized Canopy Height values estimated from cloud-to-cloud distance in the vertical (+Z) axis (Bottom).	40
FIGURE 8: Environmental noise. Flagged (grey) points have been identified as being spatially isolated with a radial distance greater than 1 m from their nearest neighbor using a local density filter.	41
FIGURE 9: Canopy Height Classes. Classified using six geometric determined class breaks within ArcMap. Each class has been adjusted to the nearest decimeter (TABLE 5).	42

CHAPTER 3.

FIGURE 10: Study site showing georeference points used to co-register MS and TLS datasets. TLS derived DTM shown with 5 m contour lines.	65
FIGURE 11: Reference data sampling locations. Six randomly generate sample locations per height regime. The northwest quadrat has few sampling points due to low field sampling accessibility. Points outside of the known height regimes were used strictly for validation of classification results.	66
FIGURE 12: Multispectral Worldview-2 Satellite Imagery. False color image shown using bands (731). Healthy photosynthetic vegetation is contrasted in red against non-vegetation surfaces.	67

FIGURE 13: HSI / NDVI1 Band Values. HUE values ranging from 0 – 360 (1). NDVI1 Values range from -1 – 1. MSB5 and MSB7 were used to generate this image (2). Intensity values range from 0 – 1 (3). Saturation values range from 0 – 1 (4).68

FIGURE 14: (TLS2) Vertical concentration of LiDAR points per raster cell. Areas of high density are indicative of vertical faces including cliffs and tree trunks.....69

FIGURE 15: (TLS3) Normalized Canopy Height Model. TLS derived vegetation height estimates of the forest canopy surface.70

FIGURE 16: (TLS4) Surface reflectance. Bare earth has a significantly greater reflective response compared to vegetation. Green vegetation reflectance is moderate to low. These difference enhance class distinctions.71

FIGURE 17: Primary canopy cover type classification results. More than 85% of the vegetative community is composed of non-native species while roughly 15% is composed of native species (TABLE 4).72

LIST OF TABLES

CHAPTER 2.

TABLE 1. Differentially Corrected GPS locations collected at each scan position. UTM NAD 83 Zone N4.....	32
TABLE 2. Multi-Station Adjustment results for each scan position. Position 4 serves as pivot point for spatial transformation.	32
TABLE 3. DTM Processing point count results for each processing step.	33
TABLE 4. nCHM Processing results. Point count effects of noise removal and height estimation steps.	33
TABLE 5. ArcMap Geometric classification results. Normalized height classes derived using ESRI geometric classification of the rasterized point cloud at 50 cm resolution. ...	33

CHAPTER 3.

Table 6. Bran-Blanquet Cover Abundance Scores. Primary canopy cover estimates for sample sites	61
TABLE 7. MS Imagery Dataset / TLS Dataset co-registration results.....	62
TABLE 8. SVM model vectors and associated attributes.	63
TABLE 9. Classification confidence and estimated coverage area. Confidence values are representative of the predicted confidence for each ROI across all segmented regions for the entire crater.	64

APPLICATIONS OF ADVANCED REMOTE SENSING TECHNIQUES FOR TERRAIN CHARACTERIZATION

THESIS ABSTRACT – Idaho State University (2015)

This thesis evaluates the use of remote sensing data fusion for classifying the primary canopy cover type of a densely vegetated crater on the Island of Molokai using terrestrial laser scanning (TLS) derived structural indices and a support vector machine (SVM) object oriented image classification. First we use TLS to derive a high density point cloud of the forest structure. Next we use a progressive filtering technique to remove vegetation in order to extrapolate the underlying terrain using a combination of mean filter thresholds (curvature, roughness, distance to nearest neighbor (D2NN)) to eliminate vegetation cover. We then derive several characteristic raster models including canopy height (CHM), canopy density (CDM) and surface reflectivity of the forest structure. Finally, we integrate these datasets into an object oriented supervised classification based on and SVM classification model. The combination of these datasets allows us to successfully differentiate between four primary canopy cover types and three soil classes amidst relatively low spectral heterogeneity. This study presents a reliable method for extracting bare earth characteristics from raw TLS generated point clouds along with a fusion workflow for modeling forest compositional traits which can reveal valuable ecological attributes associated with species dynamics for monitoring and the evaluation of various management practices.

CHAPTER 1. INTRODUCTION AND BACKGROUND

STATEMENT OF PURPOSE

The distinct physical and cultural features of Kalaupapa's historic context necessitate an inherent need for documentation. Much like the entire chain of islands in the Hawaiian archipelago, the Kalaupapa peninsula on the Island of Molokai suffers from degrading pressures imposed by exotic threats, both culturally and environmentally (Price et al. 2012, Sakai et al. 2002). The historical landscape of the Kalaupapa peninsula was once comprised of an endemically rich ensemble of vegetative communities; however, only a few remnants of this historical landscape remain (Kirch 2002). The peninsula is known to have prehistorically been a place of settlement to Hawaiian families dating back as far as A.D. 1200 as indicated by archeological evidence, making it one of the earliest recorded regions of Polynesian inhabitation (Kurashima & Kirch 2011). Post-historical evidence based on stories and legends have described conflicts between Hawaiian groups over the Kalaupapa region between A.D. 1866 – 1778 before the establishment of a leprosarium in 1865 (Kirch 2002). The establishment of the leprosarium resulted in a complete cultural disconnect for these families and is now recognized as a new era of regional stewardship, which has led to the National Park Service's interest in the preservation of its cultural landscape.

Unfortunately there has been a lack of knowledgeable documentation regarding recent dynamic changes that have progressively transpired both culturally and environmentally in the wake of a population influx beginning in the early 1800's (Greene 1985, Thomas 1995). Although the early Polynesians introduced many colonial species

for subsistence farming, clothing, shelter, boats, and tools, globalization has facilitated, to a much greater extent, similarly accelerated influences such as species introductions and increased anthropogenic exposure (McCoy 2005a). Furthermore, inadequate time for biologic stability to reach equilibrium indicates a dynamically unstable environment which threatens the integrity of past and present conditions (Kirch 2007). There is an urgent need to understand and quantify these dynamics to preserve both the cultural and physical components of these landscapes.

Like many national parks, KNHP has a great deal of both cultural and ecological resources. However, in the context of the Hawaiian culture, these resources of synonymous and intimately linked in such a way that they must ultimately be considered in together in context. Many species of vegetation are considered culturally important and have become iconic in both cultural meaning and as ecologically descriptive components of the region. Kalaupapa is considered a refuge for many threatened and endemic species of vegetation that have cultural significance to the ancient Hawaiians. In additions, there are various ornamental species which were introduced during its use as a leprosarium through missionaries and are considered monumental remnants of that era. These characteristics respectively define what is referred to as the cultural landscape of Kalaupapa.

Remote sensing approaches offer a unique advantage over conventional sampling techniques by reducing the dependence on activities which can potentially lead to further physical disturbance in highly sensitive areas (Costantino & Angelini 2013). Although satellite imagery has become an effective tool for assisting in landscape studies at large scales, these methods are typically focused on immense regions which would be difficult

to map using conventional approaches (Pu & Landry 2012). Similarly however, these methods have applications in relatively small regions where cultural and social restrictions limit the necessary access to fulfill certain research objectives.

While representing a viable approach to conducting landscape analysis on a broad scale, imagery based remote sensing techniques are still fairly limited by their ability to assess characteristics of large scale features such as terrain and forest structure. Passive remote sensing technologies inherently lack the ability to penetrate canopy layers to determine characteristics, mainly the underlying ground surface. In some scenarios, the underlying ground surface can be estimated using interpolation methods such as kriging, however these approaches are ineffective without an adequate amount of sampled ground points or visible bare earth, and are thus more applicable to large regions with sparse canopy characteristics. Furthermore, exclusive reliance on these tools for spectral classification are often met with unique challenges in areas of relatively homogenous spectral diversity or characterized by complex topography such as those on tropical islands (Clark et al. 2004, Syed et al. 2005). To address these limitations, researchers have suggested data fusion approaches which are based on multi-sensor integration of both active and passive remote sensing in an effort to overcome the individual limitations of single-sensor dependencies (Chen et al. 2005, Singh et al. 2012).

Both active and passive remote sensing technologies provide complimentary methods of retrieving information about an objects physical characteristics. LiDAR derived digital elevation models (DEM) have been used to orthorectify simultaneously captured RGB imagery to produce orthomosaics that exhibit less distortion than those produced using the traditional photogrammetrically generated digital elevation models

(DEM) (St-Onge et al. 2008). Schenk and Csathó combined LiDAR derived digital terrain models (DTM) with aerial imagery to improve automated feature extraction of buildings across urban landscapes by improving the distinguishability of objects (Schenk & Csathó 2002). By combining LiDAR products with spectral imagery, foresters can derive better estimates of stand age associated distinct canopy regions. The importance of these extrapolated datasets is far reaching in the realm of ecology by allowing more detailed examinations to be conducted while minimizing cost.

This thesis focuses on the development of a data fusion approach applied to a small yet topographically complex ecological region on the Hawaiian Island of Molokai in order to document and characterize vegetative communities and the ecological state to develop a base line interpretation complimentary to long term monitoring and management goals. Currently, there is a lack of sufficient data from which accurate canopy models can be derived, therefore our first objective is to develop a DTM of the ground surface and a subsequent canopy height model of the vegetative communities within the crater. Our second objective is to identify ecological components within the Kauhakō crater by using a data fusion approach to augment the LiDAR dataset with multispectral satellite imagery. The supplementary datasets produced through these methodologies are primarily intended to provide beneficial support to ongoing ecological surveys established by the Kalaupapa National Historic Park in Hawaii.

1. Extrapolate underlying ground surface using TLS point cloud to produce a DTM and nCHM of the Kauhakō crater.
2. Develop vegetation classification map by augmenting TLS raster products with Worldview-2 imagery to identify primary forest canopy components.

TERRESTRIAL LASER SCANNING

Terrestrial Laser Scanning (TLS) is a form of active remote sensing which can yield enhanced accuracy and higher resolution structural datasets over that of passive imaging technologies such as satellite and aerial photography (Chen et al. 2005, Papasaika & Baltsavias 2009, Kim 2007, Leeuwen & Nieuwenhuis 2010). In many ways, TLS and aerial LiDAR scanners (ALS) operate on fundamentally similar principals, however, the means through which TLS is deployed and the nature of its scanning functions make it an ideal candidate for localized uses.

The term LiDAR is an acronym for a technology most commonly referred to as Light Detection and Ranging. This technology was developed as a tool to exploit both the physical and temporal properties of light in order to infer information about distant objects. LiDAR scanners emit a precisely measured pulse of energy and record both the time stamp of emission and detected return as well as the amplitudinal signature of the returning backscatter. From this information range can be resolved from the measured time of flight using the known properties of the speed of light as it travels through a medium. This information is used to repeatedly calculate coordinates of the incident point of reflectance in 3D space in order to build what is commonly referred to as a point cloud. In addition to distance ranging, amplitudinal properties of the returning backscatter

can be used to reveal information about the surficial characteristics of a target such as their physical dimensions, orientation and reflectivity. Multiple points can be measured for each discrete pulse emitted from the scanner. As the pulse travels further from its point of origin, beam attenuation causes the laser footprint to increase. Unless an object is larger than the width of attenuation, a single pulse can result in a fractional return of the unobstructed pulse while a small remainder continues to travel and generate consecutive returns from targets along its path.

Depending upon the desired application, various LiDAR systems exist featuring varying wavelength, amplitude, and acquisition patterns. While the most common operating wavelength for scanning vegetation is around 1064nm, new emerging platforms featuring other useful wavelengths such as “green” 532 nm LiDAR with the ability to penetrate water are being rapidly adopted for bathymetric applications. In the near future, the single wavelength LiDAR systems are likely to be replaced by multispectral platforms using tunable lasers that can scan targets using a multitude of broad-spectrum wavelengths simultaneously. While LiDAR platforms operating outside the visible spectrum are harmless to the naked eye, green LiDAR is not. Depending on the wavelength and amplitude of emission, some LiDAR systems can be harmful to the eyes especially if they operate between the 400-700 nm range, thus requiring protective eyewear and limiting their use in populated areas. Deployment of LiDAR sensors can vary by application however most common systems are aerial terrestrial or mobile platforms.

TLS systems compliment the applicable uses of ALS while addressing many of the shortcomings associated with small scale applications. These systems are able to

produce significantly denser point clouds and can be rapidly deployed at more effective vantage points to maximize coverage of surfaces that would normally be occluded using ALS. Prime examples include the quantification of mass wasting events, debris falls along high relief cliff, mapping cave tunnels, and quantifying subsidence and volumetric basin capacities for watershed analysis (Barnhart & Crosby 2013, Stock et al. 2012, Kasperski et al. 2010, Buchroithner & Gaisecker 2009, Delparte et al. 2014) In the realm of ecosystem sciences, TLS has demonstrated effective use in quantifying biomass for fuel load modeling, characterizing complex terrain and the retrieval of forest structure parameters (Glenn et al. 2011, Guarnieri et al. 2009, Leeuwen & Nieuwenhuis 2010). While TLS offers an advantageous approach to sampling over conventional means, it too presents shortcomings in the form of data interpretation. Although point clouds provide intuitive descriptions of scan targets, individual points provide impartial details and must be contextually regarded by their spatial relationship to their neighbors to infer structural information. In essence, the ambiguity of point cloud geometry suggests that ancillary datasets can improve the assessment of TLS data. There is a growing body of knowledge focused on the augmentation of LiDAR datasets with multispectral imagery in an effort to avert the shortcomings associated with either technology, particularly in landscape classification and ecological research (Chen et al. 2005, Varga & Asner 2008, Schenk & Csathó 2002, Glenn et al. 2011).

MULTISPECTRAL IMAGERY

Multispectral (MS) imaging is recognized as a mature form of remote sensing that has been successfully deployed as a scientific tool for ecological research at a global scale for several decades. Beginning with film based camera systems and greatly

enhanced by the introduction of digital sensors, multispectral imaging has become a mission critical tool in the evaluation of earth systems (Morales 2012). The fundamental design of digital imaging systems allows for precise measurements of electromagnetic radiation of which indicators to various substances can be derived. Distinguishable characteristics of a surface can therefore be measured by its response to known wavelengths of light. Thus the spectral signature of an object can be used as a discriminant indicator of its physical nature. In the case of ecological research, remote sensing through multispectral imaging allows us to characterize landscapes in a biologically meaningful way indicative of species, age, senescence, and even health (Gould 2000, Latif et al. 2012, Wulder et al. 2004).

MS sensors deployed on satellite imaging systems provide unique advantages over conventional methods of sampling. Not only can they image large areas within a single image frame, they provide an accurate and convenient means of repetition allowing us to monitor dynamic earth processes over time (Boyd & Foody 2011). Furthermore, the size of the platforms enable these systems to be equipped with large high-power optics that enable high resolution mapping in multiple spectrums beyond the visible range. While the advantages of satellite remote sensing platforms are well established, there are still inherent limitations (Boyd & Foody 2011).

Many of the limitations of these systems manifest in their ability to resolve image details at decimeter scales. In conjunction with the low degree of stereo overlap provided between frames, this inhibits the capabilities of using photogrammetric solutions to develop 3D surface models at sub-m scales. For ecological research, this can affect the accuracy of classification results by as much as 30% (Nichol & Hang 2008). Although

mean surface modeling at broader scales may be beneficial to land cover research interests, the coarse resolutions and limited overlap typically provided by these sensors greatly affects the quality of producible models over small regions of interest.

DATA FUSION

There is a growing interest in the application of data fusion techniques for landscape mapping of both urban and forested regions (Boyd & Foody 2011, Singh et al. 2012, Jones et al. 2010). Data fusion as it implies involves the use of multisensory inputs to enhance modeling results by using supplemental data sources to negate the effects of inherent deficiencies common to single sensor modeling approaches (Schenk & Csathó 2002). In the realm of remote sensing, this typically implies the combination of datasets sourced from both active and passive sensing sources. While both platforms struggle to overcome the effects of occlusion, the differential trade-offs between active and passive remote sensing approaches are typically correlated to the spatial and spectral sensitivity of the equipped sensor. Consequently the enhancement of one capability inevitably results in degraded performance of the other. By incorporating a data fusion approach into methodologies focused on small scale land cover classification, improvement to both spatial and spectral resolution enabled us to conduct more intricate types of research (Chen et al. 2005).

CHAPTER 2. SPATIAL MODELING OF DENSELY VEGETATED TERRAIN WITH GEOMETRIC FILTERING TECHNIQUES USING TERRESTRIAL LASER SCANNING (TLS)

Abstract – This research used terrestrial laser scanning (TLS) to document the structural characteristics of a densely vegetated crater on the Hawaiian island of Molokai in Kalaupapa National Historic Park. A high spatial resolution (50 cm) digital terrain model (DTM) of the ground surface was derived using a filtering approach that relied on local mean curvature, roughness, and nearest neighbor approximations to remove residual noise produced by impartial ground returns. A variable kernel scale is used to remove points with a high degree of local variance. A Delaunay triangulation is then used to interpolate regional holes created by regions of prevalently identified noise. A densified point cloud is then used to estimate distances between the resulting DTM and the original dataset to model vegetative canopy heights. Height estimates were performed using a cloud-to-cloud (C2C) comparison to derive signed distance estimates exclusively in the +Z direction for all constituent points using k-nearest neighbors (kNN) clustering. The resulting point cloud is used to estimate vegetation heights and identify vegetation height regimes which may be correlated to species specific growth patterns.

INTRODUCTION

Located in one of the most isolated regions of the Hawaiian Islands, Kalaupapa National Historic Park (KNHP) is regarded for its scenic beauty and exceedingly high cultural value. The historical context of KNHP is defined by various stages of occupation that spans over 800 yrs. dating back to the discovery of the Hawaiian Islands by

Polynesian explorers (Kurashima & Kirch 2011). The chronology of the Kalaupapa peninsula can be roughly divided into three distinct eras, the first being prehistoric occupation by Hawaiians (1200 -1865), the second being its occupational use as an isolated colony for patients of Hanson's disease (1865 – 1980), and the third being the stewardship by the National Park Service (NPS) (1980 – Present) (Greene 1985). Of the many duties of the NPS, in conjunction with their obligations to the remaining patients that still reside in KNHP, is to efficiently manage the inseparable cultural and environmental resources which comprise the cultural landscape of KNHP. Due to the sensitivity of the ecological resources and the numerous archeological sites scattered throughout its boundaries, documentation and management efforts must be conducted with extreme care. Parts of the park harbor numerous rare or endangered species which can be found nowhere else on Earth (Kirch 2002). Furthermore, many of the cultural aspects of KNHP are connected to the ecological resources therefore necessitating a delicate yet efficiently sensitive approach to resource documentation.

Remote sensing approaches offer a unique advantage over conventional sampling techniques by reducing the dependence on field surveys which can potentially lead to further physical disturbance in highly sensitive areas (Costantino & Angelini 2013). Although satellite imagery has become an effective tool for assisting in landscape studies at large scales, the scope of these methods are usually limited due to insufficient spectral separability, resolution and occlusion as a result of positional disadvantage (Pu & Landry 2012). Furthermore, exclusive reliance on these tools are challenged by areas of homogenous spectral coverage such as those in closed canopy tropical forests where variations in canopy height are less detectable by conventional image based classification

approaches (Clark et al. 2004). Terrestrial Laser Scanning (TLS) is an effective form of active remote sensing which can yield enhanced accuracy and higher resolution structural geometry datasets over that of passive imaging technologies such as satellite and aerial photography (Chen et al. 2005, Papasaika & Baltsavias 2009, Kim 2007, Leeuwen & Nieuwenhuis 2010). In many ways, TLS fundamentally behaves similar to other technologies based on time of flight measurements from active sensing devices such as airborne LiDAR systems (ALS), however, the orientation of TLS data acquisition patterns enable much higher density datasets to be produced over smaller regions than by ALS. Additionally, TLS restricted to vertically stratified measurements, but as an arbitrary mix of radially oriented horizontal projections which must be considered when performing classification by order of return. Many applications relying on TLS acquired data diverge from ALS at the post processing stage based on this assumption.

In this paper we present the results of an application of TLS for the derivation of digital models representing bare earth and canopy height characteristics within a highly vegetated volcanic crater located in Kalaupapa National Park in Hawaii. Due to the density of the vegetation within this difficult to access region, derivation of spatial products characterizing the underlying ground surface are challenging. Therefore, the processes described in this research builds upon previous studies by implementing filtering approaches previously developed for use with ALS to isolate ground classified returns. We used a moving window approach to extract the lowest ground return using a 1 m kernel. However, instead using a point at the center of each window with a mean elevation value of all the neighboring points within the window, we preserved all point attributes including coordinates and eliminated all points except the point with the lowest

elevation. Next, we used a progressive filtering process based on mean curvature and roughness values to remove noise caused by vegetation to enhance the estimated ground surface. Lastly, we used a Delaunay triangulation to produce an interpolated ground surface which was then used to approximate vegetation height values. Final raster and vector products from this work are intended to be utilized by park management to identify and monitor dynamic changes in vegetation structure and forest canopy over time.

METHODS

STUDY SITE – The Kauhakō crater is located at the center of the Kalaupapa peninsula on the Hawaiian Island of Molokai (**Error! Reference source not found.**). It is characterized by a large heavily vegetated crater with a large pit in the middle. The crater is approximately 600 m wide at the rim and nearly 50 m deep (Aruch 2006). The pit in the center (Pu'u Ali'i) is the result of a source lava tube that is believed to have fed the Kauhakō caldera (Coombs & Hawke 1989). The summit of the crater rises 120 m above a centrally located lake at its center which rests at mean sea level and is topographically characterized by vegetated hanging walls and sharp cliffs around its perimeter. The Kauhakō lake situated at the center is scientifically renowned for both its estimated depth (240 m) and biophysical properties; it holds a spiritually significant meaning to Hawaiian culture and regarded as a place of great importance to the residents of Kalaupapa (Thomas 1995).

The vegetative community within the crater consists of a heavy mixture of both native and non-native species, however encroachment from non-natives species both vegetative and mammalian, is becoming a significant concern. KNHP recently began

actively managing the ungulate population by removal and construction of exclusionary fences around the perimeter of the crater in an effort to reduce browsing impacts. The western slopes are densely covered by a thicket of primarily Lantana (*Lantana camara*) ranging from 1 – 7 m tall. Java Plum (*Syzygium cumini*) has been identified throughout the crater with the highest concentration located in the south eastern region. The south west rim is lined with small groves of Ironwood (*Casuarina equisetifolia*) which drop heavy needles, consequently deterring other vegetation from growing below its canopy. The east and south rims are composed of a mixture of Wiliwili (*Erythrina sandwicensis*) and Christmas-berry (*Terebinthifolia Raddi*), the latter of which is considered to be an undesirable weed and detrimentally damaging to native forests across most of the Hawaiian Islands (Little & Skolmen 1989).

DATA COLLECTION – In order to estimate biophysical properties of the vegetative components within the crater, nCHM and DTM products were developed using TLS point clouds to estimate forest structure and detailed land cover metrics in the next chapter. The nCHM included canopy cover while the DTM provided an interpolated bare earth model of the crater. A Riegl VZ1000 TLS was used to record the unbiased structure of the crater, then later processed and filtered to derive raster products suitable for assessing vegetation height classes in the form of a normalized nCHM.

Documentation of the spatial structure of the crater was performed on August 8th, 2014 between the hours of 11:45 and 19:30 GMT-10. The scanner was positioned at six vantage points located around the crater rim (FIGURE 1). Multiple scans were performed at each location providing nearly full coverage of canopy features as well as partial yet usable coverage of the understory structures including the ground surface. At each scan

location, GPS points were collected using position averaging of occupancy times ranging from 40 - 60 minutes (Trimble GeoXH 6000). GPS solutions were then resolved using differential correction provided by the Continuously Operating Reference Station (CORS) located at Haleakala on the island of Maui (NOAA 2013). Positional offset of the laser scanner to the GPS receiving antenna was recorded to within 1 cm for direct georeferencing of the scan position data (TABLE 1).

Each scan position was environmentally unique and required precautionary placement of the scanner in order to maximize the field of view to effectively eliminate excess data collection of objects outside the scanner's optimal range. Both dense and sparse resolution scans were performed so that the entirety of the crater visible from these vantage points could be sampled. In order to mitigate occlusion problems caused by variable densities in the vegetation patterns, it was necessary to scan from a minimum of four angles, and we used six. Using natural features within the crater, scan positions were co-registered together using a combination of discrete tie-points, tie-objects, and GPS constraints. A total of 18 tie-points and 6 tie-planes were used to reduce the overall alignment error between individual scans (TABLE 2).

DATA PRE-PROCESSING – Initial processing of the TLS scan data was performed using the device's proprietary software - RiSCAN Pro (v1.8). We used the integrated Multi-Station Adjustment (MSA) tool to co-register scan positions based on a combination of GPS location and elevation point data collect during the duration of each scan. GPS positions were then transformed into UTM coordinates and exported to a common ASCII format for import into open source post processing software (EDF R&D 2015). Prior to registration, minor noise removal was required to enhance the quality of

the scan positions by removing environmental artifacts such as birds or rouge points caused by low passing clouds.

Pre-processing of environmental noise was initially performed using simple thresholds of reflectance and deviation at the RAW data level using RiSCAN. This effectively filtered out problematic points generated by erroneous returns from close-range objects while using the scanner with its long range mode of 150 Hz. Most of these points could be described by the measured waveform deviation of the recorded echo. Points consisting of relatively high deviation could be directly associated with backscatter, which at close range could be filtered using two parametric thresholds for deviation and range. We used a range-limited deviation filter of values greater than 50 within a 20 m range to eliminate most of the perceivable backscatter from the RAW scan data.

The approach used to co-register individual scan positions was on a proprietary form of iterative closest point (ICP) which used a combination of tie-points, tie-planes, and GPS positions (Reigl, 2014). Four 14.5 cm disk reflectors were used to provide reference points to scans collected within adequate range of about 400-500 m from the reflector locations. At farther ranges, horizontal spacing between the vertical scan lines was inadequate to record a sufficient number of points on the surface of the reflectors. Furthermore, the presence of obstructions in the peripheral views of the scan positions inhibited the stable placement of reflectors in locations that could be used from multiple scan positions. Consequently, strategic alignment using reflector targets became impractical based on this method alone. We used a mix of clearly recognizable features from conjugate scan locations as alignment surfaces. Features were chosen based on their

resilience to motion caused by prevailing winds as well as an association with a discrete range of reflectance values making them easily identifiable (Habib et al. 2008).

Simultaneous georeferencing and co-registration in RiSCAN Pro was performed using a combination of point and vector surface features within the scan data along with positional GPS data. GPS scan positions were used to initially georeference the scanner locations using a fuzzy boundary equal to the size of the positional dilution of precision (PDOP). Tie planes were used for planar alignment based on features with low linear variation such as fence posts while tie-points were used to anchor each point cloud around common points. Points recorded along the edge of a fence post were ideal for determining planar alignment since they theoretically fall along a linear plane.

We performed a chain alignment using a subset of the six scan positions to fix our initial georeference positions and bearing. Scan positions were constrained using the PDOP value reported by the GPS device while the bearing was determined by conjugate tie-points in each scan. A proprietary form of an iterative closest point (ICP) procedure known as a Multi-Station Adjustment (MSA) was used to perform a constrained adjustment of the scan positions while minimizing the overall RMS of the tie-objects (RIEGL 2014). Scanner orientations were then locked relative to each other and offset using the measured distance from the GPS antenna to the base of the scanner. This translation resulted in an improved alignment of 4 cm using 18 tie-points and 6 tie-objects (TABLE 2). All scan positions were then exported to ASCII format using the NAD83 UTM Zone 4N coordinate system. Reflectance values were then normalized to a ranging of 0 to 1 and stored as 32-bit floating point integers to ensure both backward and

forward compliance with ASPRS standards for all versions of the LAS file format (ASPRS 2011).

TERRAIN PROCESSING AND NORMALIZATION – CloudCompare was selected for DTM processing based on its robustness, abilities to handle large point clouds, a well-supported mix of interchangeable file formats, and a well-documented toolset. For each subsequent point cloud produced by the progressive curvature and roughness filtering workflow outlined in this chapter, a numerical identifier will designate a new filtering step, ie: $C_0 - C_9$. The full point cloud (C_0) produced from high resolution scans of all six positions consisted of nearly 640 million points. Therefore a filter was used to identify and remove points that met redundancy criteria to produce a more manageable dataset that still provide adequate detail (FIGURE 3). This method used a moving window approach to analyze the localized distances to all neighboring points within a defined radius (Guarnieri et al. 2009). These distances were weighted to determine which points in the neighborhood were closest to the gravitational center of the local cloud and flagged as non-duplicate. Duplicate points that were within the defined radius were then flagged and removed keeping the point closest to the gravitational center. We defined our search radius to 10 cm, which was just slightly greater than the approximate error reported through the co-registration process to produce our primary working dataset (C_1).

In order to assess extent of ground coverage from the TLS scans, C_1 was first height grid filtered to preserve the lowest elevation values within each grid cell. By observing the effects of scale dependency on regional coverage using the lowest elevation filter, a local scale of 5 m was selected as base resolution for estimating a suitable starting point for ground surface interpolation. The general approach was to height filter the point

cloud using the lowest elevation points at a grid size that minimized the amount of surface variability caused by environmental noise while maximizing resolution and detail. We decided to use a subsampling method as opposed to a resampling method to preserve point coordinates instead of creating a new regularized cloud with points at the center of each grid cell. After several iterations, we determined that a grid resolution of 1 m² provided the greatest balance between noise and topographic fidelity to produce the 2nd iteration of our refined point cloud (C₂).

We began by performing a curvature analysis using a 2 m kernel which provided a means of identifying the range of curvature associated with noise points at the smallest possible scale. Mean curvature estimation is based upon an average of six quadratic polynomials fit to the six nearest neighbors (EDF R&D 2015). The first technique for removing false ground points was to use a fine scale curvature analysis. With a mean spacing of 1 m, the smallest possible kernel size to use for curvature analysis must be 2 m in order to ensure sufficient neighbors exist from which to approximate a local least squared plane (LSP). After computing the mean curvature for each point, the top five percent of the curvature values were histographically identified and removed at a threshold value of 18 cm to produce C₃.

Post curvature analysis revealed that small clusters of spatially isolated points still existed after the first pass of filtering. Therefore, a density filter using distance to nearest neighbor (D2NN) values was used to thin out the majority of these remaining groups of points. A histogram of nearest neighbor (NN) values revealed that 99% of the constituent points were within at least 1.5 m of a neighboring point. A threshold value of 99% was

used to filter the top 1% of points having greater than 1.5 m of distance between the nearest neighboring point to produce C₄.

To remove more points without inadvertently removing critical points from the higher relief terrain, a low pass roughness filter was used to produce C₅. Roughness is described as the distance a point lays from a localized plane defined by the three nearest neighbors. The benefit of this filter was that it was especially useful for removing single points that had significantly larger elevation deltas than their neighbors. In this case, a 4 m kernel would be composed of roughly 10-15 points depending on point distribution extremes of the terrain. This was effective for isolating narrow spikes in elevation throughout the dataset. A threshold value was used to filter out all points with roughness values greater than 1m. Another curvature filter was then applied to eliminate residual points using an increased kernel size, which was less sensitive to the influence from micro-topography. A 5 m kernel was chosen after comparing the results of various sizes between 2-10 m. Points were filtered that had a curvature value greater than 10 cm or roughly the upper 1% of all curvature values to produce C₆.

A statistical outlier removal (SOR) operator was then applied using 10 nearest neighbors with a threshold of 1 SD to produce C₇. This effectively removed rogue points located in regions of low point density, a characteristic common to sub-canopy points (Guarnieri et al. 2009). The success of this filter used at this stage in the processing can be attributed to reduction of surrounding noise points. The SOR filter first computed the mean and SD distances between a point and its neighbors. Outliers that do not meet the parameterized criteria were then removed (Rusu & Cousins 2011).

To improve height estimation between the estimated ground surface and vegetation, holes in the point cloud needed to be filled using an interpolated surface and then resampled for distance computation (C_8). This was accomplished using a Delaunay triangulated surface with a maximum distance threshold of 30 m to ensure cliff lines and large holes would be closed. The final point cloud (C_9) was then produced by resampling the triangulated surface at a point density of 100 pts/m².

CANOPY HEIGHT MODEL PROCESSING AND NORMALIZATION – A cloud to cloud (C_2C) distance comparison was performed between the final point cloud (C_9) and the unprocessed point cloud (C_1). For the interest of height estimation in the presence of sub-canopy features with varying degrees of spatial density, a kNN estimate from 15 neighbors was used to compute cloud distances between the two points ($C_1 - C_9$). Distances were computed for each axis separately enabling the discrimination of vertical offset exclusively along the vertical (Z) axis as opposed to using the estimated normal vector (FIGURE 7).

Following the assignment of normalized heights to point cloud C_1 , a Connected Components clustering filter process was used to eliminate any residual points produced by atmospheric scattering over the duration of each scan (EDF R&D 2015). Typically, these types of points were spatially isolated and exhibit a broad range of reflectivity values: thus identification using this tool was fairly simple and highly efficient using parameters of octree level 10 [68 cm] and a minimum point count of 2 to produce C_{1N} . This step was saved for last to ensure that it did not result in removal of potential ground points until estimated height values have been assigned (FIGURE 8).

Noise was identified in the raw dense point clouds where sub canopy echoes did not fully resolve or follow characterization patterns compared to surface canopy regions.. These points were identified as being spatially isolated and insufficient at distinguishing class membership. These were quickly filtered out using a region selection of 10 or greater sample points, then filtered by mean and standard deviation of both reflectance and deviation values. Although the majority of points identified using these parameters were legitimate noise, a small portion of sub canopy points were also distinguishable by these parameters. This filtering method was sufficient for removing noise despite the false positives since the percentage of false positives was considered negligible, constituting less than 1% of the dataset as indicated by the histotrophic view of the pre-filtering effect on the dataset.

In order to output the point cloud as a raster, one final step had to be performed to ensure success due to software limitations. Both the final ground classified point cloud (C_9) and the cleaned vegetation height estimated point cloud (C_{1N}) were cloned, grouped, merged and then exported to both raster and point cloud products. Raster products were exported with a 50 cm ground sample distance (GSD) using maximum height values per grid cell. Point clouds were exported to LAS and ASCII formats with a relative density of 10 cm. Both elevation and normalized height values were stored as scalar fields. Point cloud C_{1N} should be considered a nCHM as it incorporated the underlying spatial structure from both canopy and sub canopy features.

RESULTS

The resulting ground classified point cloud (C_9) characterizes an interpolated estimation of the ground surface beneath a dense forest canopy. The change in point populations between subsequent filtering steps illustrates the effect of chosen filter thresholds for each type of analysis with emphasis on the preservation of points may potentially be representative of the true ground surface (TABLE 3). The first filtering steps used to reduce the overall point cloud density to a manageable size while still maintaining fidelity at a 10 cm scale effectively removed 92% of the overall points. Although the original point cloud (C_0) had relative point densities that could be used to resolve stem level details, it hindered processing speeds and made it difficult to address the overall management of the dataset.

The initial height grid filtering process successfully identified 87.9% (12,928 m²) of the ground surface using a 1 m² grid cell size (FIGURE 5). Curvature filters were the most effective method of removing noise from the subsequent point clouds. The first curvature filter used a 2 m kernel size with a threshold of 18 which accounted for the retention of 86% of the remaining cloud. The second filter used a 5 m kernel and a 10 cm threshold that was far more effective than the prior Roughness filter which relied on a 4 m kernel with a 1 m threshold. The final noise filter applied to (C_6) resulted in a point population that was reduced by 99.7% compared to the pre-noise filtered cloud (C_1).

The vegetation point clouds were processed in a similar method as to preserve as many points as possible that may be representative of vegetation structure. Other than duplicate point removal which was performed on the raw point cloud (C_0), the only filtering process that was performed on the vegetation point clouds after height values

had been assigned was the removal of floating noise attributed to atmospheric refraction of the laser pulse. This step resulted in a visually effective yet negligible loss of 0.05% of the point cloud (TABLE 4). This step was necessary to ensure that the resulting raster products derived from this cloud were not influenced by spurious points that existed above the vegetative canopy. The rasterized nCHM revealed a stratification of six distinct vegetation height classes throughout the primary canopy region (FIGURE 9). We used an ESRI geometric classification in ArcMap to identify break values using normalized heights (TABLE 5).

EMPIRICAL ERROR ESTIMATES – The resulting ground surface point cloud (C_9) is estimated to have an empirically observed error of approximately 50 cm with a SD of 30 cm. The dominant source of measured error was the GPS positions used to georeference the six scan positions which had PDOP values of roughly 30 cm each (TABLE 1). Although this was significantly reduced using the MSA co-registration approach, we resampled all raster products to 50 cm to match that of existing image products (FIGURE 6).

DISCUSSION

This study demonstrated the use of TLS sampling techniques to estimate vegetation heights in a region dominated by dense forest canopy. The robustness of these methods for extracting DTM information from either sparse or dense scan data improves the amount of area that can be analyzed in comparison to ground based sampling techniques, it also compliments in-situ methods of sampling by eliminating inherent risks in which manual sampling methods may be inadequate or difficult to perform due to access restrictions.

The chosen grid resolution of 1 m sufficiently provided a balance between noise and terrain detail, which was then used to extract the lowest elevation point within each grid cell while maintaining spatial locality. Furthermore, sub-sampling the point cloud as opposed to resampling effectively preserved point coordinates without introducing estimation errors whereby the original point coordinate was used instead of placing a point at the cell center. Grid values greater than 1 m also worked, however the aim of the technique was to find the optimal grid size that could be managed with noise filtering. Grid values smaller than 1 m resulted in a cloud that was fully dominated by spurious points creating a significantly more difficult dataset to clean in order to isolate ground returns.

Noise filtering using roughness and curvature were highly effective at eliminating falsely classified ground returns which were estimated to compose roughly 12.1% of the total area extracted using the initial gridded filtering approach. In both instances, if there was a lack of sufficient neighboring points within the specified kernel size, points were flagged invalid. This was especially useful at identifying extreme outliers, however, it was not particularly conducive to preserving definition along boundary regions or where occlusion had produced holes in the gridded point cloud. The D2NN filter was better at remove these same outliers without falsely removing points due to the lack of neighbors. Instead this worked well for removing points that had any number of neighbors that were outside the range of the neighborhood threshold.

It was discovered that the order in which each filter was applied had a significant effect on the noise identification results. By using an iterative approach beginning with a small kernel size and progressively working towards a large scale kernel, the efficiency

of these tools was optimized by enhancing the detection rate between each filtering pass. The small scale kernel is more sensitive in the presence of lots of noise, this is why it is the first filter to be processed. Larger scale filters end up underestimating local values at the beginning of the filtering process but tend to improve as noise is gradually reduced. Less points were evaluated with high mean values when large filters were used at the beginning of the process which resulted in having to redundantly use them later towards the end of the process to produce good results.

Both of these tools functionally complement each other; curvature worked well for identifying points in regions dominated by dense noise whereas roughness worked well at preserving surface definition and micro topography in topographically complex regions such as cliff lines. The curvature filter seemed to provide a more aggressive approach at identifying noise as opposed to roughness, especially in regions containing small clusters of noise points. This is likely due to a larger minimal set of points used to evaluate curvature (6 pts) as opposed to roughness (3 pts).

SOURCES OF ERROR – While the factory reported accuracy of the laser scanner is about $\sigma = 8$ mm with a beam divergence of 30 mm at a range of 100 m, the majority of intrinsic scanner error is believed to be attributed to a “one size fits all” scan range setting combined with dynamic changes occurring in the environment during the duration of each scan epoch (RIEGL 2014). The scanner was successfully able to sample distances further than required for the study site, however a comparison between two range settings of differing horizontal density revealed that long range scanning frequencies typically tended to produce a greater amount of noise. The two main sources were extremely close range objects and possibly aerosols both atmospheric and depositional on feature

surfaces. These two phenomenon were easily mitigated using the scanners proprietary RiSCAN software to perform filtering based on waveform deviation, which described how the energy of a return compared to the initial pulse as it left the scanner (RIEGL 2014). Longer waveforms like those used for long range scanning have a tendency to produce false returns from close range objects, creating a smearing effect along edges of scan features. In densely vegetated environments, this effect can be highly prominent. The combination of deviation filtering of the raw cloud combined with the removal of duplicate points during the pre-processing phase made this smearing effect negligible and inconsequential in the final results.

Motion of scanned objects was another source of error. Winds and low density clouds caused both scattering effects and ghosting as a result of moderate to severe motion in tree tops and the passing effects of moisture. Both effects were reasonably compensated for through post processing and had very little effect on the accuracy of the final products.

Alignment error, although present, was minimized during the MSA alignment which used a chain optimized algorithm similar to the *LoopClosing* algorithm proposed by (Wulff 2010) for minimizing alignment error in photogrammetric datasets. Alignment error introduced by tie-objects such as dead branches and metal fence posts could be seen as an effect of locational uncertainty resulting from the given scan density, the amount of surface area covered by the horizontal scan spacing, and the degree of stability exhibited by each object, all of which were considered to be negligible considering the accuracy of our georeferencing positions.

The majority of the filtered processing in this study involved sample point elimination defined by statistical thresholds. Areas of the DTM characterized by extremely high relief such as cliff zones inherently suffer most from interpolated errors. In the context of this study, however, the vantage point of each scan position made lateral sampling of adjacent cliffs easily feasible due to the relative absence of vegetative obstructions. In these regions, cliff lines were more susceptible to filtering techniques performed during the DTM extraction process associated with the degree of curvature and roughness filtering performed, therefore, the values used for these filters may not be applicable to other sites without slight modification to the filtering thresholds matched for other terrain types.

COMPARATIVE ALTERNATIVES – In comparison to other methods of LiDAR point classification such as ENVI LiDAR or LAStools, the methods outlined in this research performed better when it terms of both the amount of initial ground point estimation and the removal of noise introduced by vegetation. Tools such as LAStools and ENVI LiDAR provide the convenience of scripted batch processing, however these tools were designed using proprietary algorithms and were designed primarily for ALS applications. Neither of these tools were able to adequately process this particular dataset, regardless of the degree of parameterized tuning. The methods proposed in this study produced superior results and bring the convenience of being freely available and capable of being ran of a wide range of systems. The developmental roadmap for the software environment used in this research outlines command line scripting and batch processing integration without using a graphical interface, thus making our methods easily adaptable to future research projects.

The beneficial aspects the approaches offered by this research to KNHP are 1) The ability to spatially document sensitive regions without physical sampling which may be destructive. 2) Quantification of topographic and vegetative characteristics in difficult to access regions. 3) These methods are repeatable, scalable and can be broadly integrated with various types of datasets or provide supplemental enhancements to conventional survey practices.

ACKNOWLEDGMENTS

The authors would like to acknowledge Erika Stein Espaniola (KNHP Superintendent) and Dr. Paul Hosten (KNHP Terrestrial Ecologist) for their support and contributions. In addition would like to acknowledge Dr. Nancy Glenn (Professor) and Lucas Spaete (Boise State University) for their training efforts in the operation and deployment tactics using terrestrial laser scanning equipment. Funding for this project was provided through the Great Basin Cooperative Ecosystem Studies Unit, National Park Service (Cooperative Agreement No.: P11AC8R001).

LITERATURE CITED

- ARUCH, S., 2006. *Appendix A: Haleakala National Park resource overview*, Fort Collins, Colorado.
- ASPRS, 2011. *LAS SPECIFICATION VERSION 1.4 - R13*, Bethesda, Maryland.
Available at: http://info.asprs.org/society/committees/standards/LAS_1_4_r13.pdf.
- CHEN, L., T. CHIANG, AND T. TEO, 2005. Fusion of LIDAR data and high resolution images for forest canopy modelling. *In 26th Asian Conference on Remote Sensing and 2nd Asian Space Conference*. p. 7, Ha Noi, Vietnam.
- CLARK, D.B., J.M. READ, M.L. CLARK, A.M. CRUZ, M.F. DOTTI, AND D.A. CLARK, 2004. Application of 1-m and 4-m resolution satellite data to ecological studies of tropical rain forests. *Ecol. Appl.* 14: p.61–74.
- COOMBS, C.R., AND B.R. HAWKE, 1989. Kauhako Crater and Channel, Kalaupapa, Molokai, Hawaii: A Terrestrial Analog to Lunar Sinuous Rilles. *Twent. Lunar Planet. Sci. Conf.* 20: p.1095–1096.
- COSTANTINO, D., AND M.G. ANGELINI, 2013. Production of DTM quality by TLS data. *Eur. J. Remote Sens.* 46: p.23.
- EDF R&D, T.P., 2015. CloudCompare. Available at: <http://www.cloudcompare.org/>.
- GREENE, L.W., 1985. Exile in paradise: The isolation of Hawai'i's leprosy victims and development of Kalaupapa settlement, 1865 to present. [Denver] Branch Planning, Alaska/Pacific Northwest/Western Team, U.S. Dept. Inter. Natl. Park Serv. Denver Serv. Cent.p.728.
- GUARNIERI, A., A. VETTORE, F. PIROTTI, AND M. MARANI, 2009. Filtering of TLS Point Clouds for the Generation of DTM in Salt-Marsh Areas. XXXVIII: p.293–298.
- HABIB, A. F., A. P. KERSTING, Z. RUIFANG, M. AL-DURGHAM, C. KIM, AND D.C. LEE, 2008. Lidar strip adjustment using conjugate linear features in overlapping strips. *Int. Arch. Photogramm. Remote Sens. Spat. Inf. Sciences* 37: p.385–390.
- KIM, S., 2007. *Individual tree species identification using LIDAR-derived crown structures and intensity data*. University of Washington.
- KIRCH, P. V, 2002. From the “cliffs of Keolewa”to the “sea of Papaloa”: an archaeological reconnaissance of portions of the Kalaupapa National Historical Park, Moloka ‘i, Hawaiian Islands. *Ocean. Archaeol. Lab. Spec. Publ.*

- KURASHIMA, N., AND P. V KIRCH, 2011. Geospatial modeling of pre-contact Hawaiian production systems on Moloka'i Island, Hawaiian Islands. *J. Archaeol. Sci.* 38: p.3662–3674.
- LEEUWEN, M., AND M. NIEUWENHUIS, 2010. Retrieval of forest structural parameters using LiDAR remote sensing. *Eur. J. For. Res.* 129: p.749–770.
- LITTLE, E.L.J., AND R.G. SKOLMEN, 1989. Common forest trees of Hawaii (native and introduced) - *Corynocarpus laevigatus*. USDA Agric. Handb. No. 679p.1–2.
- NOAA, 2013. CORS, National Geodetic Survey. Available at: <http://www.ngs.noaa.gov/CORS/> [Accessed September 15, 2013].
- PAPASAIKA, H., AND E. BALTSAVIAS, 2009. Fusion of LiDAR and Photogrammetric Generated Digital Elevation Models. *In Proc. ISPRS Hannover Workshop on High-Resolution Earth Imaging for Geospatial Information, Hannover, Germany.* pp. 2–5, Citeseer.
- PU, R., AND S. LANDRY, 2012. A comparative analysis of high spatial resolution IKONOS and WorldView-2 imagery for mapping urban tree species. *Remote Sens. Environ.* 124: p.516–533.
- RIEGL, 2014. User's Manual for RIEGL VZ-1000 V-Line 3D Terrestrial Laser Scanner.
- RUSU, R.B., AND S. COUSINS, 2011. 3D is here: Point Cloud Library (PCL). *In Proceedings - IEEE International Conference on Robotics and Automation.* pp. 1–4, Shanghai: IEEE. Available at: <http://pointclouds.org/>.
- THOMAS, E.D., 1995. The cliffs of Kalaupapa. *Wilderness Environ. Med.* 6: p.346–347.
- WULFF, R., 2010. Image-Based 3D Documentation in Archaeology. p.10.

TABLE 1. *Differentially Corrected GPS locations collected at each scan position. UTM NAD 83 Zone N4*

Adjusted Scan Position	LAT (m)	LONG (m)	Elevation (m)	VDOP (m)	HDOP (m)	Std Dev
Position 0	711178.42 7	2344074.74 0	105.449	0.4	0.2	0.24
Position 1	711419.06 9	2344380.44 4	126.376	0.2	0.1	0.16
Position 2	711435.99 6	2344555.21 8	119.002	0.2	0.2	0.42
Position 3	711402.80 0	2344633.06 9	116.959	0.7	0.4	0.18
Position 4	711326.31 5	2344577.22 5	120.622	0.4	0.3	0.18
Position 5	710937.48 9	2344221.06 5	124.106	0.2	0.1	0.14
Mean error:				0.28	0.2	0.22

TABLE 2. *Multi-Station Adjustment results for each scan position. Position 4 serves as pivot point for spatial transformation.*

Scan Position	ΔX (m)	ΔY (m)	ΔZ (m)	Δ Roll ψ	Δ Pitch θ	Δ Yaw ϕ	links	Remarks
Position 0	0.152	-0.01	-0.045	0.001	-0.011	-0.026	25	
Position 1	-0.007	0.01	-0.009	0.073	-0.013	-0.016	15	
Position 2	-0.017	-0.011	-0.122	0.015	0.004	-0.009	27	
Position 3	-0.631	1.733	42.328	1.295	4.153	-0.145	12	
Position 4	0	0	0	0	0	0	14	Locked
Position 5	0.094	-0.096	-0.19	-0.014	0.018	-0.017	27	
Error (Std Dev) [m]:	0.0492							

Number of observations used for calculation:

Tie-points: 18

Tie-objects: 6

TABLE 3. *DTM Processing point count results for each processing step.*

Filter Step [Threshold]	Δ Points Count	Δ Residual Points	Δ Points (%) $C_{(N-1)}$
(C ₀) Unfiltered cloud	0	638,580,640	
(C ₁) Remove Duplicate Pts [10 cm]	-588,875,522	49,705,118	-92.2
(C ₂) Height Grid Filter [1 m]	-49,450,480	254,638	-99.5
(C ₃) Curvature [2 m,18]	-35,086	219,552	-13.8
(C ₄) D2NN [1.5 m]	-2,305	217,247	-1.0
(C ₅) Roughness [4 m,1 m]	-5,431	211,816	-2.5
(C ₆) Curvature [5 m,10]	-81,592	130,228	-38.5
(C ₇) SOR [10,1]	-2,811	127,417	-2.2
(C ₈) Delaunay Mesh	254,622 (faces)	127,417	-99.7 (C ₁)
(C ₉) Mesh Resampled [100 pts/m]	2,907,137		+95.6

TABLE 4. *nCHM Processing results. Point count effects of noise removal and height estimation steps.*

Filter [Threshold]	Δ Points Count	Δ Residual Points	Δ Points (%) $C_{(N-1)}$
(C ₀) Unfiltered cloud	0	638,580,640	
(C ₁) Remove Duplicate Pts [10 cm]	-588,875,522	49,705,118	-92.2
(C _{1N}) C2C Evaluation [15, Z]	0	49,705,118	0
(C _{2N}) CC SOR [50,3]	-26,564	49,678,554	-0.05

TABLE 5. *ArcMap Geometric classification results. Normalized height classes derived using ESRI geometric classification of the rasterized point cloud at 50 cm resolution.*

Height Class	Class Adjustment (m)
Bare Earth	0 – 0.6
Low Shrubs	0.6 – 1.7
Tall Shrubs	1.7 – 3.6
Small Trees	3.6 – 6.9
Medium Trees	6.9 – 12.9
Tall Trees	12.9 – 23.6

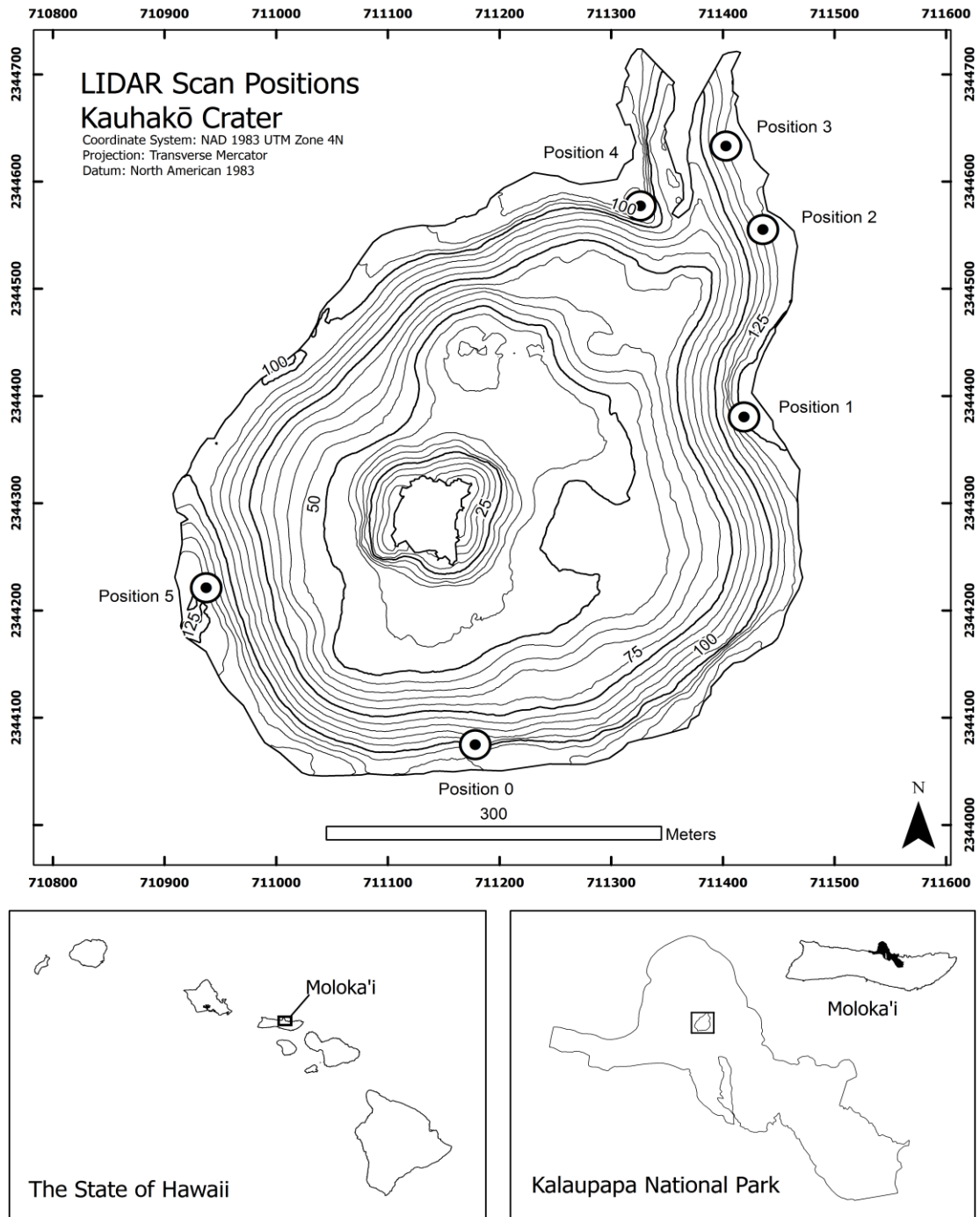


FIGURE 1: Scan locations at the Kauhakō crater study site. GPS positions were collected using a Trimble GeoXH 6000. Contours produced from resulting DTM product with 5 m spacing.

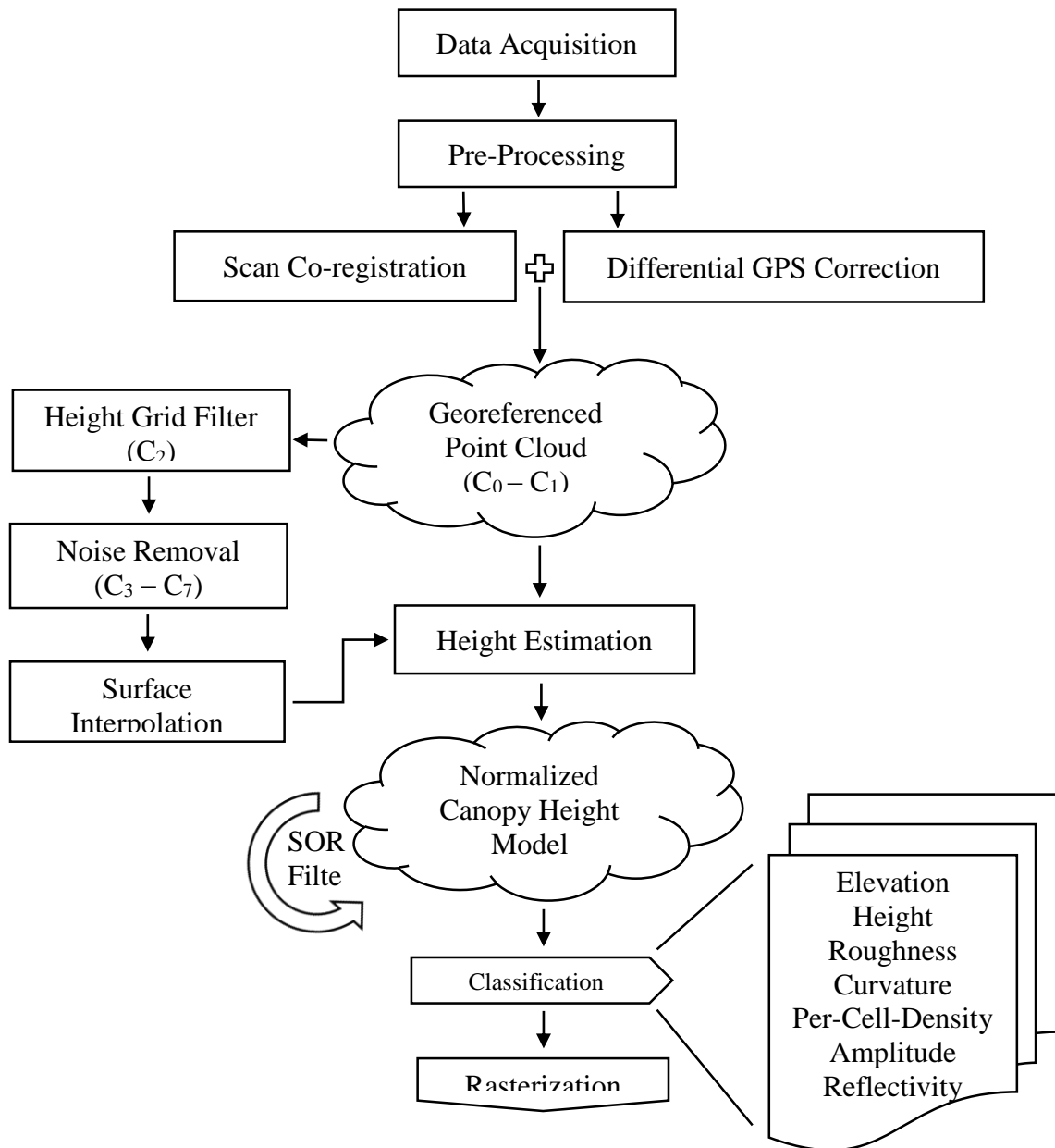


FIGURE 2: Classification workflow for TLS point cloud processing and derivative products.

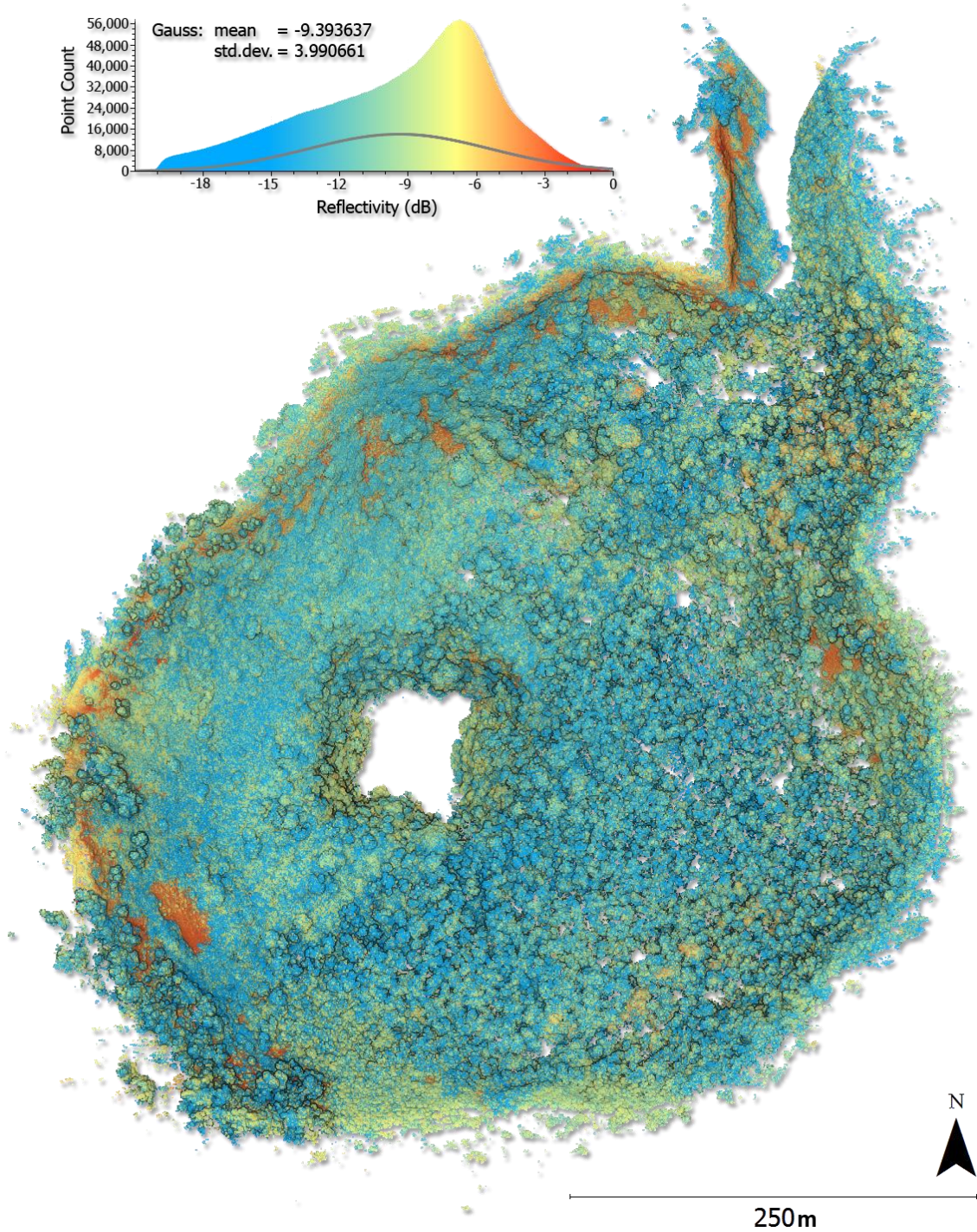


FIGURE 3: Sparse point cloud consisting of roughly 49 million points. Duplicate points have been removed with an average sample spacing of 10 cm. Color scale is indicative of surface reflectance. Healthy vegetation is distinctly less reflective than bare earth.

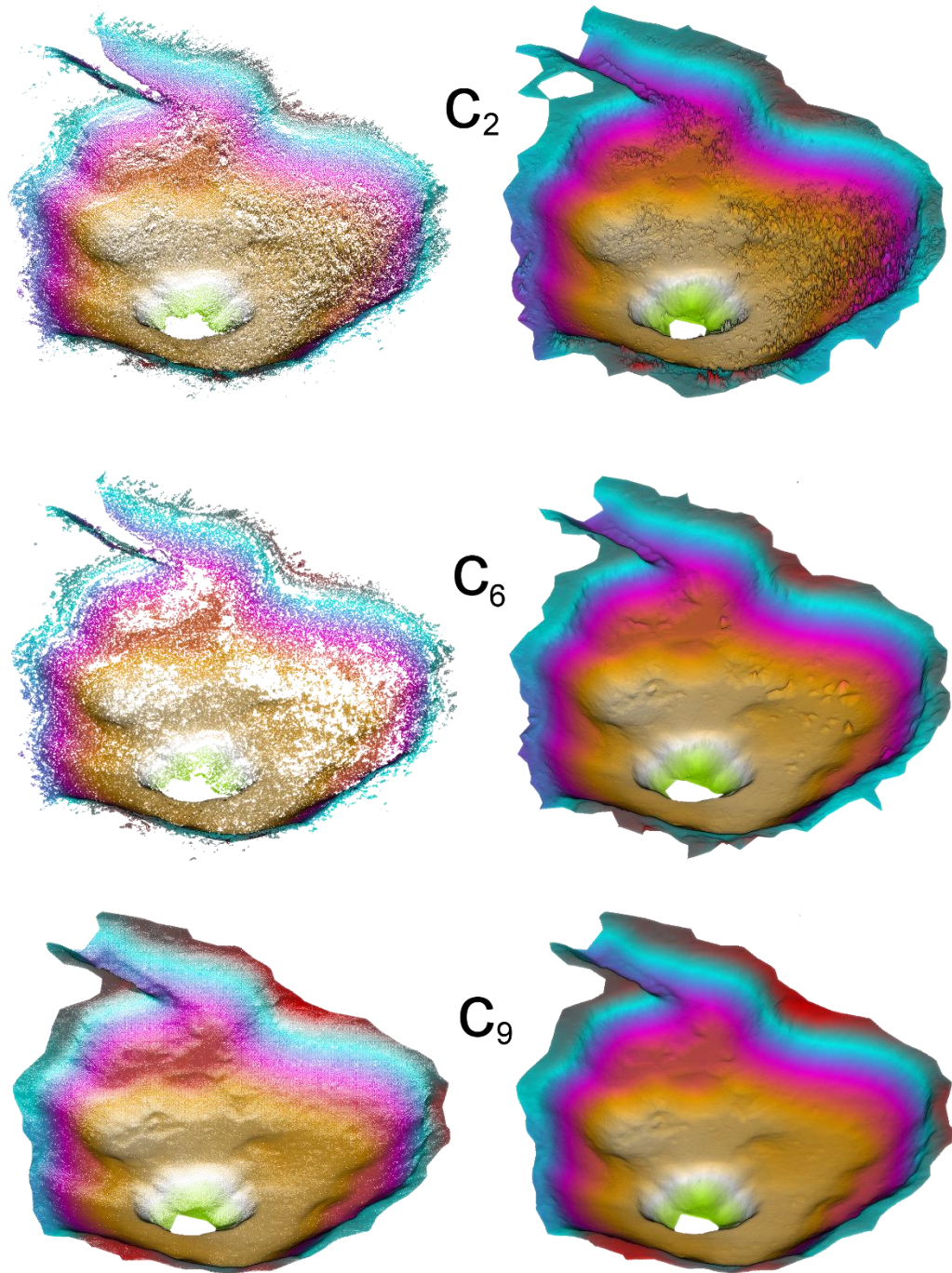


FIGURE 4: Height grid filter 1m (C_2). Result of noise removal using curvature, roughness, and nearest neighbor statistics (C_6). Final DTM result: Post SOR filtering, Delaunay mesh resampled to 100 pts/m (C_9).

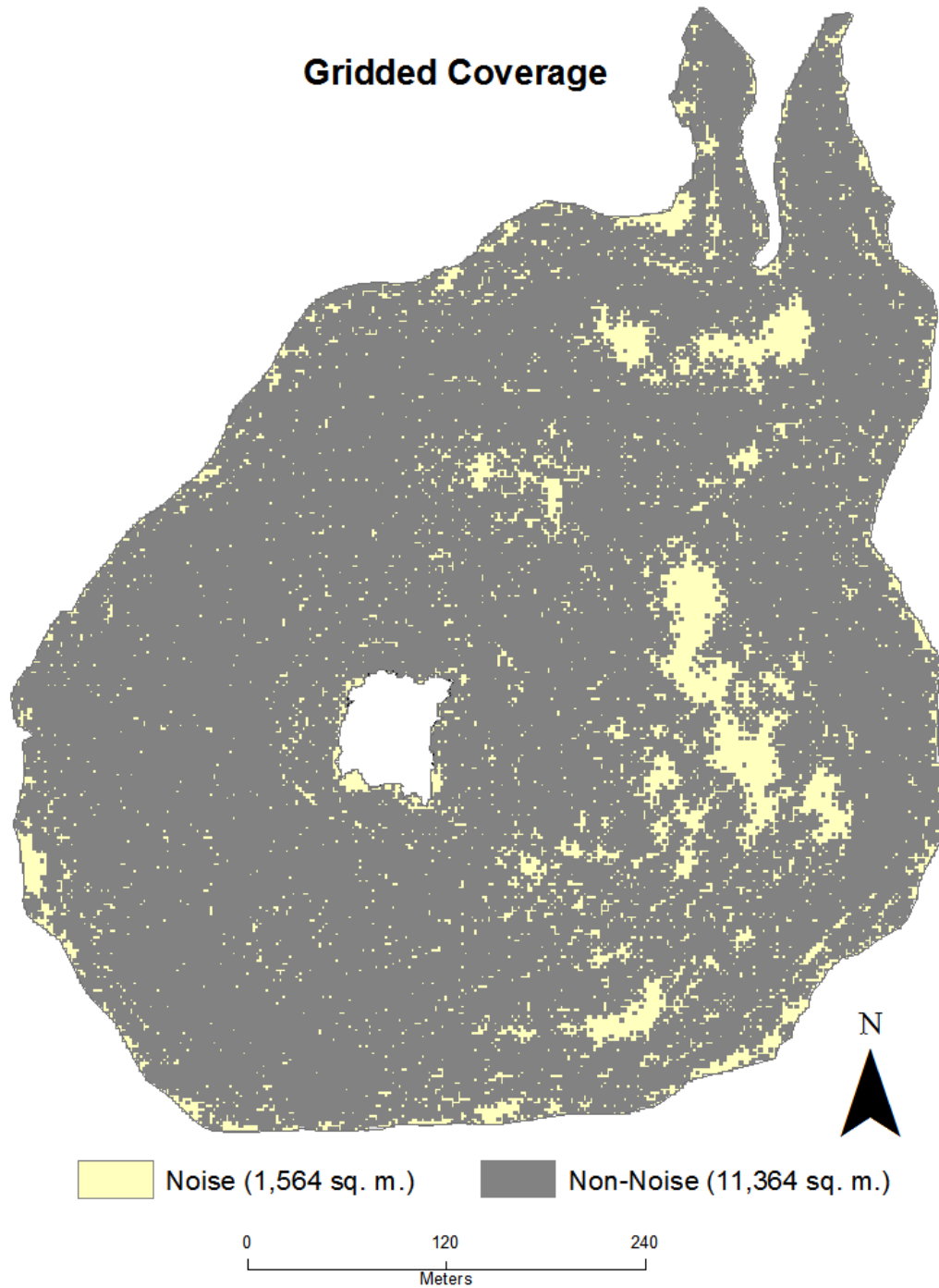


FIGURE 5: Coverage map showing areas defined as non-noise vs. areas that were classified as noise, cleaned then interpolated using Delaunay triangulation.

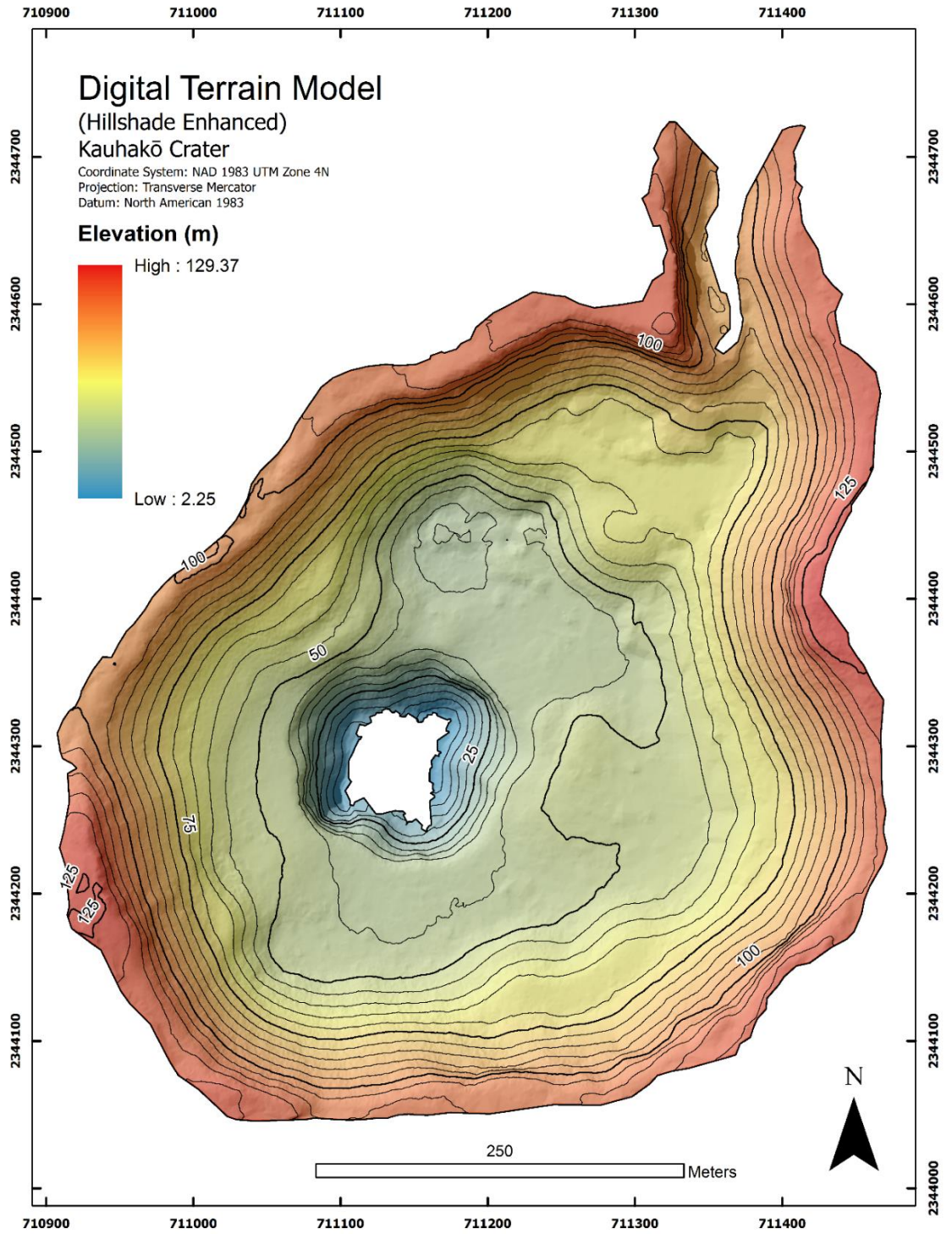


FIGURE 6: Rasterized DTM produced from (C₉). The resulting product has a 50 cm GSD with 5 m minor contour lines and 25 m major contour.

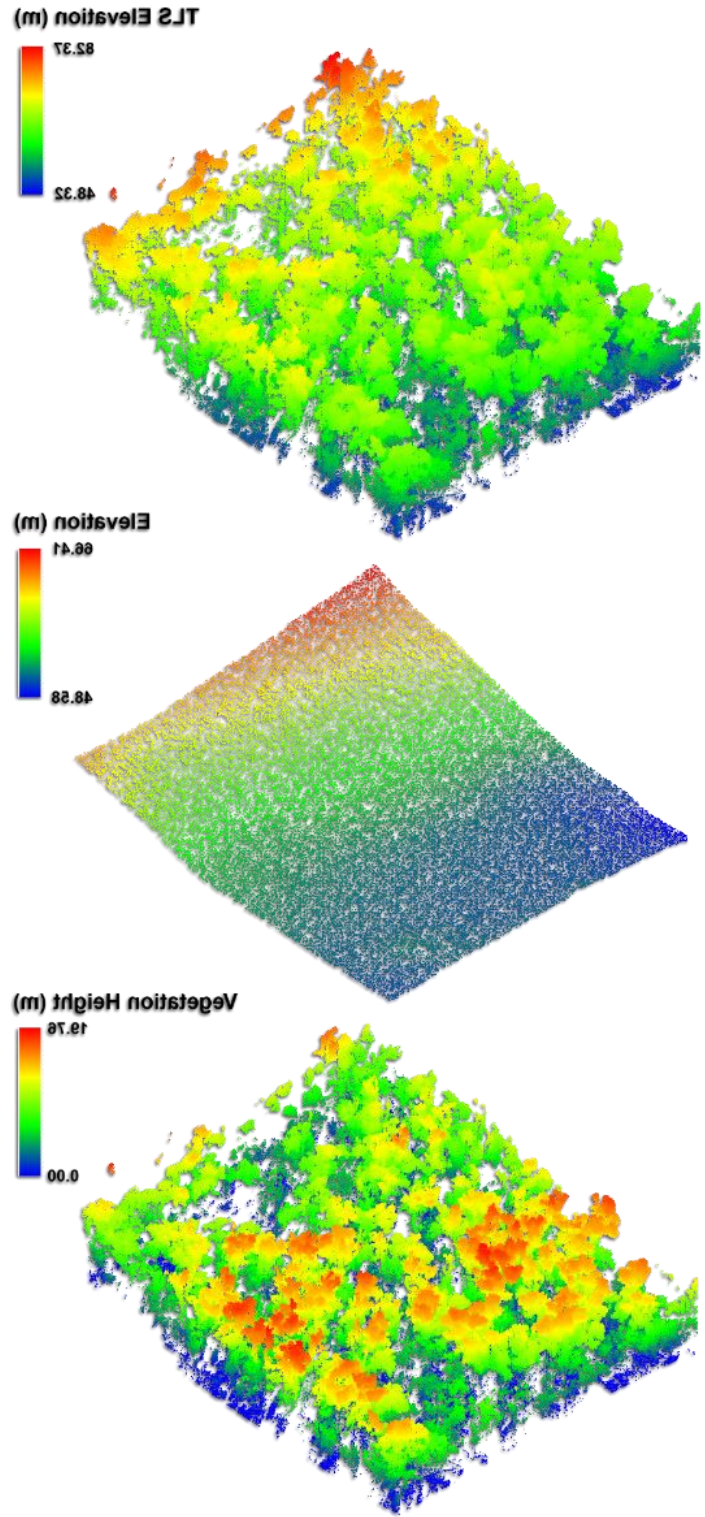


FIGURE 7: Comparison between estimated elevation values. TLS derived feature elevations (Top). Estimated elevation values for filtered ground surface (Middle). Normalized Canopy Height values estimated from cloud-to-cloud distance in the vertical (+Z) axis (Bottom).

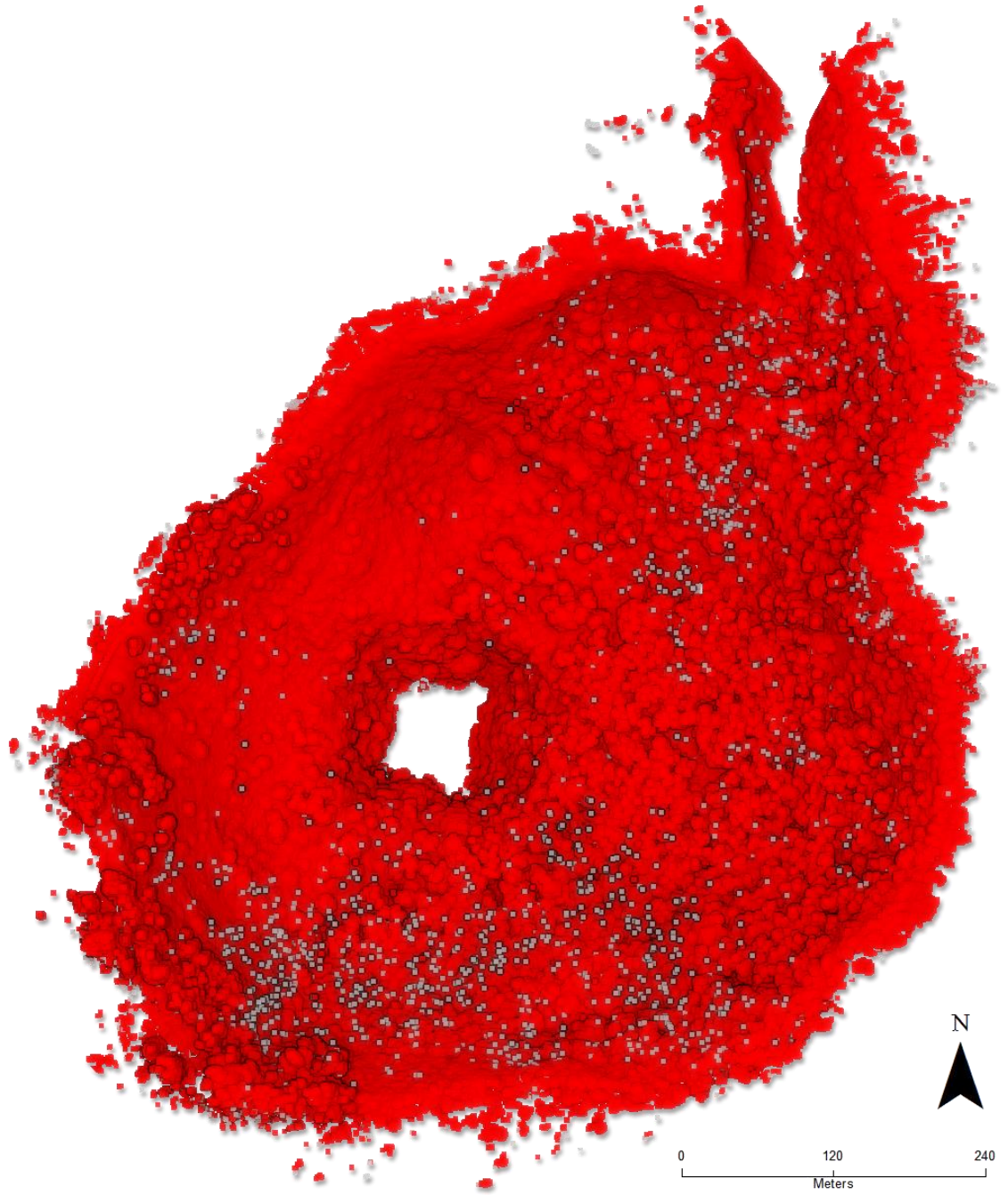


FIGURE 8: *Environmental noise. Flagged (grey) points have been identified as being spatially isolated with a radial distance greater than 1 m from their nearest neighbor using a local density filter.*

Canopy Height

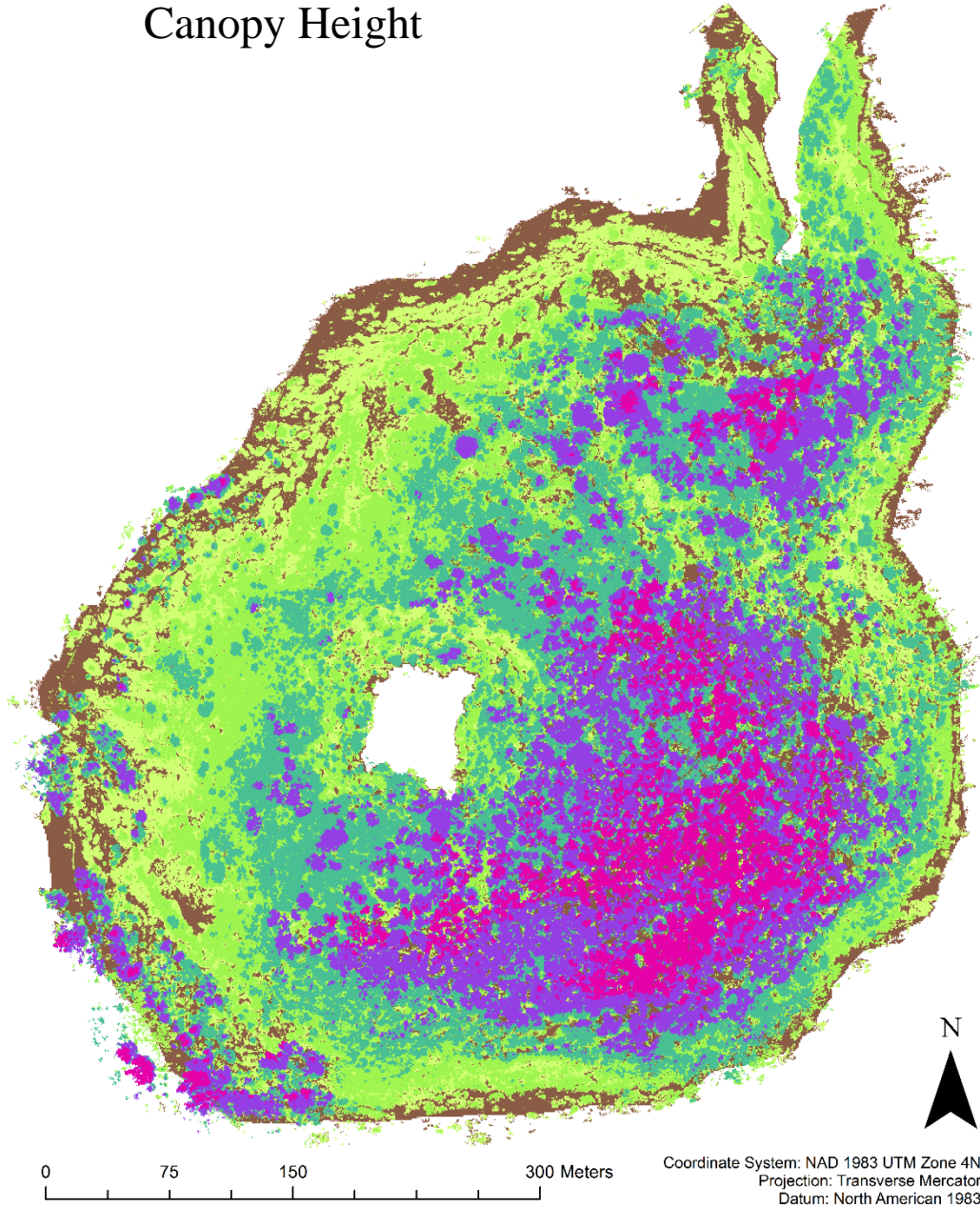


FIGURE 9: *Canopy Height Classes. Classified using six geometric determined class breaks within ArcMap. Each class has been adjusted to the nearest decimeter (TABLE 5).*

CHAPTER 3. FOREST CLASSIFICATION USING TERRESTRIAL LIDAR ENHANCED WORLDVIEW-2 MULTISPECTRAL IMAGERY

Abstract – Canopy cover type modeling is a critical aspect of ecosystem monitoring. Ecological descriptions derived from remote sensing approaches provide informative metrics characterizing ecosystem dynamics which are highly useful in landscape management. This research focuses on a data fusion approach using LiDAR and Multispectral (MS) satellite imagery to estimate forest cover types in a densely vegetated and culturally rich region of Hawaii. Spectral indices derived from MS imagery are augmented with structural attributes provided by Terrestrial Laser Scanning (TLS) datasets and integrated using a support vector machine (SVM) classification model to estimate primary cover regimes. The results indicate that this modeling approach can successfully be used to quantify canopy cover by primary cover type, thus supporting a data fusion approach as a valuable tool for conservation and ecosystem monitoring.

INTRODUCTION

Like much of the entire chain of islands in the Hawaiian archipelago, the landscape integrity of the Kalaupapa peninsula on the Island of Molokai suffers from degrading environmental pressures. The historical landscape of the Kalaupapa peninsula was once comprised of an endemically rich ensemble of ecological communities; however, only a few remnants of this historical landscape remain. The peninsula is known to have prehistorically been home to Hawaiian families dating back as far as A.D. 1200 as indicated by archeological evidence, making it one of the earliest recorded regions of Polynesian inhabitation throughout the island chain. Post-historical evidence based

on stories and legends have described conflicts between Hawaiian groups over the Kalaupapa region between A.D. 1866 – 1778 before the establishment of a leprosarium in 1865 (McCoy 2005b). The establishment of the leprosarium resulted in a complete cultural disconnect for these families that is now recognized as a new era of stewardship, led by the National Park Service, focuses attention on the preservation of Kalaupapa National Historic Park's (KNHP) cultural landscape.

While ongoing research efforts strive to document a continuum of features in an effort to preserve the cultural landscape of the region, there exists deficiencies in the bodies of knowledge regarding recent dynamic changes that have progressively transpired both culturally and environmentally in the wake of a population influx beginning in the early 1800's (Greene 1985, Thomas 1995). Although the early Polynesians introduced many colonial species for subsistence farming, as well as clothing, shelter, boats, and tools, globalization has facilitated, to a great extent, similarly accelerated influences such as species introductions and increased anthropogenic exposure (McCoy 2005a). Furthermore, inadequate time for biologic stability to reach equilibrium indicates a dynamically unstable environment which threatens the integrity of past and present conditions (Kirch 2007). There is an urgent need to understand and quantify these dynamics to preserve both the cultural and physical components of these landscapes.

Remote sensing approaches offer a unique advantage over conventional sampling techniques by reducing the dependence on activities which can potentially lead to further physical disturbance in highly sensitive areas (Costantino & Angelini 2013). Although satellite imagery has become an effective tool for assisting in landscape studies at large

scales, the scope of these methods are usually limited due to insufficient spectral *separability*, resolution and occlusion as a result of positional disadvantage (Pu & Landry 2012). Furthermore, exclusive reliance on these tools are often met with unique challenges in areas of homogenous spectral diversity such as closed canopy regions such as those found in tropical regions where variations in canopy height are less detectable by conventional image based classification approaches (Clark et al. 2004).

Support Vector Machine (SVM) learning algorithms have consistently demonstrated effective uses in MS image based classification of tropical forest regions for the identification of rare and endangered species as well as clusters of invasive species populations (Pouteau et al. 2012, Immitzer et al. 2012). Furthermore, SVM has demonstrated improved performance in studies using WV2 imagery when combined with LiDAR data as opposed to exclusive classification based on spectral attributes (Jakubowski et al. 2013). SVM operates by first projecting descriptive support vectors such as spectral attributes into a higher dimensional feature space. A kernel function is then used to determine the best fitment of these vectors to a hyperplane in order to determine which range of inputs provide optimal separability for class membership assignment.

In this paper we present the results of an applied data fusion approach to estimate the descriptive range of primary canopy cover types within a highly vegetated volcanic crater located in Kalaupapa National Historic Park in Hawaii. Due to relatively low heterogeneity of the spectral characteristics of the vegetative community, a remote sensing data fusion approach is used to effectively enhance canopy cover estimates using remote sensing approaches. Multispectral (MS) imagery acquired by the WorldView-2

(WV2) satellite was processed using all eight spectral bands. Imagery was spatially subset then used to generate spectral, textural and geometric attribute images using co-occurrence measures commonly used to vegetation analysis (Normalized Difference Vegetative Index, Intensity and Saturation)) (Kim et al. 2011). Due to provisional limitations common to satellite sensing platforms in their ability to resolve vertical estimates of surfaces geometry, TLS data was used as ancillary input to enhance the WV2 dataset by providing structural information (Normalized Canopy Height Model (nCHM), Reflectance, Per-Cell-Density (PCD), and Elevation) (Johansen et al. 2007). Combinations of vegetative and structural descriptors were then used in conjunction with training regions to segment and classify image space using a supervised method of support vector machine (SVM) analysis in an ENVI image processing environment. The resulting model prediction is validated using reference data which is compared against confidence predictions for each cover class region. This research is intended to assist landscape managers in establishing baseline condition assessments, develop effective monitoring protocols, and support informative decision making.

METHODS

STUDY SITE – The Kauhakō crater is located at the center of the Kalaupapa peninsula on the Hawaiian Island of Molokai (FIGURE 10). It is composed of two nested craters, the larger outermost being the remains of a volcanic caldera, and the small inner crater (Pu'u Ali'i) being remnant of the source vent (Coombs & Hawke 1989). The combined area of the two is roughly 0.25 km² with an overall maximum elevation of 120 m above MSL at the southwest side of the crater rim. This crater is moderately round characterized by steep walls and cliffs with a lake situated at mean sea level in the center

of the basin. The majority of the crater is vegetated with exceptions where heavy erosion prevents soil accumulation near the base of cliff faces and outside the crater rim where there are very few wind breaks. The lake is scientifically renowned for its geophysical properties with an estimated depth of over 200 m; additionally it is held with spiritual significance to the Hawaiian culture and of great importance to the residents of Kalaupapa (Thomas 1995).

Primary canopy cover within the crater is comprised primarily of a dense mixture of invasive species. A few remnant communities of native species coexist in the sub-canopy regime, however fierce competition has greatly reduce the native species richness throughout the entire crater. Regardless of this fact, the area is still regarded as one of the most pristine native forests zones on the Kalaupapa peninsula. A dense thicket of Lantana (*Lantana camara*) ranging from 1 – 7 m tall grows along the entirety of the crater rim where it is heavily mixed with Christmas Berry (*Schinus terebinthifolius*), the latter of which is considered to be an undesirable weed and exceedingly harmful to native forests across the majority of the Hawaiian Islands (Little & Skolmen 1989). Java Plum (*Syzygium cumini*) has been identified throughout the crater, however the tallest specimens ranging from 7 – 24 m have been predominantly identified in the south east region. The south west rim is lined with small groves of Ironwood (*Casuarina equisetifolia*). Originally introduced after the establishment of the leprosarium, this iconic species drop heavy needles, consequently preventing the establishment of other vegetation by the release of allelopathic compounds. There are known groves of native Wiliwili (*Erythrina sandwicensis*) that exist along the west rim and in the center of the

crater just south of Pu'u Ali'i. This species is significantly important to the Hawaiian culture and is an important health indicator in native Hawaiian Dry Forests.

Classification of forest types was performed using a data fusion approach by integrating datasets derived from both MS satellite imagery and a terrestrial laser scanner (TLS). These datasets were used to derive vegetation indices based spectral, textural, and geometric attributes. Multispectral (MS) imagery acquired by the WorldView-2 (WV2) satellite was processed using all eight spectral bands. Imagery was spatially subset then used to generate spectral, textural and geometric indices using co-occurrence measures commonly used to vegetation analysis (Normalized Difference Vegetative Index, Intensity and Saturation)) (Kim et al. 2011). Due to provisional limitations common to satellite sensing platforms in their ability to resolve vertical estimates of surfaces geometry, TLS data was used as ancillary input to enhance the WV2 dataset by providing structural indices (Normalized Canopy Height Model (nCHM), Reflectance, Per-Cell-Density (PCD), and Elevation) (Johansen et al. 2007). Combinations of vegetative and structural indices were then used in conjunction with training regions to segment and classify image space using a supervised method of support vector machine (SVM) analysis in an ENVI image processing environment.

DATA COLLECTION – A WV2 image of the Kalaupapa National Park was acquired on November 19, 2012 which was comprised of eight MS bands and one panchromatic band. Each MS band had a spatial resolution of 2m, was radiometrically corrected to radiance values, dynamically range adjusted (DRA) and delivered in 8-bit WV2 format (.TIL) images. The panchromatic band was delivered in the same format with a 50cm ground sample distance (GSD). The MS imagery was then pan-sharpened (PS) in ENVI

5.2 using a Gram-Schmidt Pan-Sharpening method which has been regarded in the remote sensing industry as one of the premier method of sharpening very high spatial resolution (VHR) MS imagery (Maurer & Street 2013).

TLS scanning was performed on August 8th, 2014 between the hours of 11:45 - 19:30 using a Riegl VZ1000 to record the unbiased structure of the crater then later processed to derive products suitable for assessing vegetation height classes in the form of an nCHM and PCD datasets. In addition, a spectral product characterizing surface reflectance in the 1550 nm wavelength was derived to further assist in the identification of relevant features. As described in Chapter 2, each TLS product was rasterized by extrapolating the highest elevation point within a 50 cm window, then exported with a GSD of 50 cm, matching the resolution of the pan-sharpened MS imagery.

Reference data were collected using survey points acquired on March 19-18, 2015. A Trimble GeoXH 6000 was used to collect GPS locations for each surveyed site. GPS solutions were then resolved using differential correction provided by the Continuously Operating Reference Station (CORS) located in Honolulu on the island of Oahu (NOAA 2013). In accordance with establish KNHP practices, site surveys were conducted using the Braun-Blanquet Cover Abundance (BBCA) methodology which is regarded as a practical and efficient means of describing phytocoenosis (Poore 1955). For each of the six height regimes identified from the TLS dataset, six navigation waypoints were generated for a total of 36 sampling sites (FIGURE 11). For each waypoint, two constraint parameters were used to balance the quantitative distribution of points across each height regime. 1) A minimum point spacing of 20 m was used to prevent over clustering of sample locations 2) The minimal area of a region must be greater than or

equal to 16 m² to be included in the pool of possible areas a point can be generated for. We used 4 m x 4 m quadrats to survey each waypoint location with the quadrat center being marked with a new GPS point upon arrival. Within each quadrat, three canopy regimes were evaluated by a KNHP staff ecologist and used to determine cover abundance. Primary canopy being the uppermost canopy regime, secondary being the next major canopy regime followed by a ground level canopy. Although more canopy classes likely exist, we determined that these three are the most relevant to the task of spectral classification using the MS dataset as well as establishing overstory dominance. For the purpose of image classification, the primary canopy was used to identify training regions and test our model efficiency. Cover abundance scores were assigned to each species identified within the three canopy regimes. Values of 1 – 5 and (-) were assigned for each species with respect to their associated cover percentage or absence within each regime (**Error! Reference source not found.**). The most abundant cover types were then used as descriptors for forest type and the derivation of classification training regions.

IMAGERY AND LIDAR CO-REGISTRATION – Upon comparison between the MS image and the TLS datasets, there was immediate evidence that the two data sources exhibited subtle distortional differences throughout their frames of reference. Therefore it was necessary to adjust one or the other datasets to achieve a better co-registration prior to image analysis. We chose to rectify the TLS dataset to improve alignment with the WV2 dataset. Although the TLS dataset had a lower spatial error than reported for the MS imagery, we chose to rectify the TLS dataset to ensure that future analysis using satellite imagery based on a similar spatial reference standard would be preserved.

ArcMap was used to georeference the TLS dataset to the WV2 imagery using a set of control points based on distinct features in each dataset. These control features primarily consisted of isolated vegetation patches, rocky out-crops and prominent canopy features of old growth forest. Control points were randomly distributed throughout the study site as to minimize transformational bias (FIGURE 10). An “Adjust” type spatial transformation was chosen to rectify the TLS dataset to the WV2 imagery which provided a much better alignment over the second best option: 3rd Order Polynomial (TABLE 7). In total, 58 control points were used.

IMAGE SEGMENTATION – Image processing using the Feature Extraction (FX) module in ENVI 5.2 can be divided into two phases. The 1st involves edge detection which creates segmentation boundaries that delineate image space into meaningful regions, then a merger of small segments into more homogenous clusters based on mean spectral attributes. The 2nd step involves classifying each segmented region by its spectral, textural and geometric attributes. Image segmentation in the EX module uses an approach similar to those used in hydrologic modeling based on a filling approach that first identifies the lowest values throughout an image, then identifies regions with statistically similar values defined by applying an aggregate threshold (Xiaoying 2012, Roerdink & Meijster 2000). Next, regions are merged together based on similarity between mean spectral values. The merge algorithm iteratively computes the Euclidean distance between adjacent regions, then evaluates their similarity using a Full Lambda Schedule. As long as the merging cost is less than our defined threshold, adjacent regions are merged (Robinson et al. 2002). This step doesn’t necessarily require the same input

bands as used in the initial segmentation, but may in fact use any combination of available bands in an effort to improve the merge results.

We determined that the use of the three most spectral separated bands (731) from the satellite dataset worked best for edge detection with the inclusion of synthetic images for Saturation, Intensity and NDVI1 to highlight differences between vegetation and bare earth (FIGURE 12). The NDVI1 image was generated using a normalizing band-ratio between MSB7 (NIR1) and MSB5 (RED) which demonstrated a slight improvement in feature distinction over the standard NDVI approach using MSB6 (RED EDGE) and MSB5 (RED) when used in densely vegetated regions exhibiting relatively high levels of evapotranspiration (Nouri et al. 2013, Upadhyay et al. 2013). Hue, Saturation and Intensity (HSI) have been indicated to improve classification accuracy in some cases by as much as 15% in studies pertaining to evapotranspiration, therefore we used standard color space bands (532) to produce HSI images (FIGURE 13) (Laliberte & Rango 2008).

IMAGE CLASSIFICATION – Image classification was performed using a supervised object oriented approach which required a selection of training regions of interest (ROI) and attributes derived from spectral information to define class descriptors. Eight ROI class types were derived by targeting ecotone boundaries (distinguishable transition boundaries between adjacent but heterogeneous vegetative communities), bare earth types, and exclusionary shadow regions (Pouteau et al. 2011). Attributes were automatically assessed by the image analysis tool using the most ideal endmember separability. Of the eight class types, four represented dominant vegetation, three represented varying forms of bare earth, and one represented unclassifiable regions dominated by shadows where spectral signatures were diluted by illumination

discrepancies. Bare earth classes were divided into Types 1-3 depending on the degree of mineral decomposition. Bare earth Type-3 was a special mix of both types 1 and 2 that were indistinguishable due to solar glare in the WV2 image. Attributes were assessed per region using combinations of spectral, textural and geometric criteria from various combinations of band inputs (TABLE 8).

PREDICTION MODELING – We used an SVM modeling approach to predict species distributions based on our eight types of ROI. As suggested by (Pouteau et al. 2011) and widely supported by similar research, a Radial Basis Function kernel type can be applied to a robust mix of applications and requires only a few parameters to be defined. We used a Gamma value of 0.30 which is close to the inverse of the amount of computed attributes used (8) to assign class memberships. A Penalty Parameter was used to control the trade-off between enforcement of training errors and rigid margins along class boundaries. Possible values range from 0.00 – 100.00 with the higher values resulting in a more accurate model at the cost of misclassification. Logically a value of 100.00 should only be used in the case of perfect training data. We used a penalty value of 90 to balance class reassignment effects during our region selection. A threshold parameter of 40 to restrict the results of classification by limiting the probability at which regions were assigned an unclassified value.

RESULTS

CLASSIFICATION ATTRIBUTES – MSB1 (Coastal) had the highest occurrence (8) across all computed attributes. TLS1 (elevation) was used in all four attributes computed against MS bands, but was not used for any textural attributes. TLS2 (PCD) was used in all four MS attributes, and two textural attributes: range and entropy (FIGURE 14). TLS3

(nCHM) was the most useful of the LiDAR products, having seven of the eight classification attributes computed for it (FIGURE 15). TLS4 (reflectance) was used in three spectral attributes and two textural attributes (FIGURE 16).

HSI bands were moderately useful across a range of computed attributes. Hue was only determined to be useful for one spectral attribute (Spectral Std. Dev), however it was used to compute two textural attributes (range and variance). Saturation was used to compute two pairs of spectral and textural attributes. Intensity had the highest rate of inclusion of the three HSI images across seven computed attributes NDVI1 was only used to compute four attributes; three spectral and one textural (TABLE 8).

Of all the computed attributes, spectral mean (SM) and spectral minimum (SMN) were the most useful with 15 of the 16 bands being used. Textural mean (TXM) had the second highest inclusion rate in which all eight MS bands were computed for. Spectral std. deviation (SSD) was the least useful with regard to MS bands, however it was computed for all four of the commonly used TLS bands.

COVER TYPE CLASSIFICATION – As indicated by both our reference data and validated by the model prediction, forest canopy cover is dominantly composed of two primary species, *Schinus terebinthifolius* and *Syzygium cumini*, both of which are considered highly invasive in Hawaii (FIGURE 17). *Syzygium cumini* was the most dominant cover type (32.9%) covering roughly 0.82 km². *Schinus terebinthifolius* was the second most common cover type comprising 20.2% or roughly 0.51 km². Both native vegetation types contributed a combined total of less than 10% by cover. *Erythrina sandwicensis* had a predicted cover contribution of 5.7% while *Lantana camara* was estimated at 3.3%. In total, nearly 86% of all vegetation within the crater is non-native.

Since the majority of *Lantana camera* occurs just outside the rim of the crater, we estimate only 9% of the primary cover type within the crater is composed of native vegetation, mainly *Erythrina sandwicensis* (TABLE 9).

Bare earth was estimated to have a combined total exposed cover contribution of 19.7%. Most of this is accounted for by soil deposits along the northwest rim of the crater between adjacent patches of *Schinus* and *Lantana*. Exposed cliff line along the northern and southern rims accounted for roughly 9% of the exposed bare earth total. Highly reflective bare earth is a special class in that it is an indiscriminant amount of both Type 1 and Type 2 soil classes (3.6%).

Regions covered by shadows posed an issue to the completeness of our survey. A good portion of our reference data points landed in regions of significant shadowing, thus we could not use these points to verify class memberships. By classifying portions of our imagery according to the effects of shadowing, we could potentially estimate the proportional subset of our data that would result in heavy misclassification had these regions been included with rest of the high visibility ROIs.

CLASSIFICATION CONFIDENCE – Confidence results for our predicted regions were higher than anticipated. Confidence prediction were determined by ENVI with respect to each image segment and its associated similarity to the computed attributes for each ROI. The mean confidence across all cover classes was 0.54 – 0.75. The range of standard deviations across classes confidence values was narrow (0.18 – 0.26) indicating consistent estimates for all cover types (TABLE 9).

DISCUSSION

IMAGE SEGMENTATION – During segmentation, the combination of MS bands (731), NDVI1 and HSI values were the most effective at delineating ecotone boundaries. When ancillary TLS data was included as a segmentation parameter, the segmentation image produced sparse anomalous regions which seemed to be an effect of coverage discrepancies between the satellite and TLS datasets, therefore the inclusion of TLS data was reserved strictly as attribute data during the classification process.

The regions generated by the edge segmentation were then merged using a mean value threshold from the same set of segmentation bands. We found that a value of [Merge: 81.0] provided the best discriminant results between subtle spectral variances in small regions. Moreover, this value avoided excessive aggregation of large regions that shared similar mean spectral populations. Our aim was to not overly segment the image while accurately merging visibly identifiable canopy components.

TRAINING AND CLASSIFICATION – Not all species found in the region could be mapped due to the influence of spectral similarities and inherent limitations of the spectral and spatial sensitivity of the satellite sensor and in many instances, low species abundance. Among prominently occurring cover types, Ironwood (*Casuarina equisetifolia*) was deliberately excluded from classification based on the inability to produce an exclusive class without significant scene wide misclassification. We believe this is due to similarities between the computed indices which closely resemble the two primary cover types (*Syzygium cumini* and *Erythrina sandwicensis*). Furthermore, the misclassification of this species resulted in a class split between the primary cover types indicating that ROIs used for this class would have overlapped with the distinguishing

characteristics of the primary cover types. Other less abundant species such as Kukui (*Aleurites moluccanus*) and Bread Fruit (*Artocarpus altilis*) although present, were omitted from this study due to low abundance and localized occurrences, furthermore, the occurrence of these species are believed to be anthropogenic derived and non-self-propagating under the pressures of the dominant cover types.

While classification confidence values indicate consistent estimates across all classes, there are clearly a few prominent regions of misclassification. The majority of misclassification seems to be occurring in regions where shadows dilute the intensity of the spectral signal. The inadequacy of spectral signals from the MS imagery was too low to differentiate between class memberships resulting in a classification split between primary cover types. Therefore we had to create a shadow class to improve class wide estimates.

In conclusion to this research, we found strong supporting evidence that forest canopy cover classification using TLS and MS satellite imagery in a data fusion modeling approach can be quite effective. The outlined method not only demonstrates a robust alternative to field sampling, it establishes a foundation upon which future research can built upon to improve ecosystem monitoring and develop better management protocols.

ACKNOWLEDGMENTS

The authors would like to acknowledge Erika Stein Espaniola (KNPH Superintendent) and Dr. Paul Hosten (KNPH Terrestrial Ecologist) for their support and contributions to this work. Funding for this project was provided through the Great Basin Cooperative Ecosystem Studies Unit, National Park Service (Cooperative Agreement No.: P11AC8R001).

LITERATURE CITED

- CLARK, D.B., J.M. READ, M.L. CLARK, A.M. CRUZ, M.F. DOTTE, AND D.A. CLARK, 2004. Application of 1-m and 4-m resolution satellite data to ecological studies of tropical rain forests. *Ecol. Appl.* 14: p.61–74.
- COOMBS, C.R., AND B.R. HAWKE, 1989. Kauhako Crater and Channel, Kalaupapa, Molokai, Hawaii: A Terrestrial Analog to Lunar Sinuous Rilles. *Twent. Lunar Planet. Sci. Conf.* 20: p.1095–1096.
- COSTANTINO, D., AND M.G. ANGELINI, 2013. Production of DTM quality by TLS data. *Eur. J. Remote Sens.* 46: p.23.
- GREENE, L.W., 1985. Exile in paradise: The isolation of Hawai'i's leprosy victims and development of Kalaupapa settlement, 1865 to present. [Denver] Branch Planning, Alaska/Pacific Northwest/Western Team, U.S. Dept. Inter. Natl. Park Serv. Denver Serv. Cent.p.728.
- IMMITZER, M., C. ATZBERGER, AND T. KOUKAL, 2012. Tree Species Classification with Random Forest Using Very High Spatial Resolution 8-Band WorldView-2 Satellite Data. *Remote Sens.* 4: p.2661–2693.
- JAKUBOWSKI, M., W. LI, Q. GUO, AND M. KELLY, 2013. Delineating Individual Trees from Lidar Data: A Comparison of Vector- and Raster-based Segmentation Approaches. *Remote Sens.* 5: p.4163–4186.
- JOHANSEN, K., N.C. COOPS, S.E. GERGEL, AND Y. STANGE, 2007. Application of high spatial resolution satellite imagery for riparian and forest ecosystem classification. *Remote Sens. Environ.* 110: p.29–44.
- KIM, M., T.A. WARNER, M. MADDEN, AND D.S. ATKINSON, 2011. Multi-scale GEOBIA with very high spatial resolution digital aerial imagery: scale, texture and image objects. *Int. J. Remote Sens.* 32: p.2825–2850.
- KIRCH, P. V, 2007. Hawaii as a model system for human ecodynamics. *Am. Anthropol.* 109: p.8–26.
- LALIBERTE, A, AND A. RANGO, 2008. Incorporation of texture, intensity, hue, and saturation for rangeland monitoring with unmanned aircraft imagery. *In GEOBIA Proceedings.* p. 4/C1.
- LITTLE, E.L.J., AND R.G. SKOLMEN, 1989. Common forest trees of Hawaii (native and introduced) - *Corynocarpus laevigatus*. *USDA Agric. Handb. No.* 679p.1–2.

- MAURER, T., AND N.Y. STREET, 2013. How To Pan-Sharpen Images Using the Gram-Schmidt Pan-Sharpen Method – a Recipe. ISPRS Hann. Work. 2013 XL: p.21–24.
- MCCOY, M.D., 2005a. The development of the Kalaupapa field system, Moloka'i Island, Hawai'i. *J. Polyn. Soc.* 114: p.339–358.
- MCCOY, M.D., 2005b. The Lands of Hina: An Archaeological Overview and Assessment of Kalaupapa National Historical Park, Moloka'i.
- NOAA, 2013. CORS, National Geodetic Survey. Available at: <http://www.ngs.noaa.gov/CORS/> [Accessed September 15, 2013].
- NOURI, H., S. BEECHAM, S. ANDERSON, AND P. NAGLER, 2013. High spatial resolution WorldView-2 imagery for mapping NDVI and its relationship to temporal urban landscape evapotranspiration factors. *Remote Sens.* 6: p.580–602.
- POORE, M.E.D., 1955. The Use of Phytosociological Methods in Ecological Investigations: I. The Braun-Blanquet System. *J. Ecol.* 43: p.226–244.
- POUTEAU, R., J.-Y. MEYER, AND B. STOLL, 2011. A SVM-based model for predicting distribution of the invasive tree *Miconia calvescens* in tropical rainforests. *Ecol. Modell.* 222: p.2631–2641.
- POUTEAU, R., J.-Y. MEYER, R. TAPUTUARAI, AND B. STOLL, 2012. Support vector machines to map rare and endangered native plants in Pacific islands forests. *Ecol. Inform.* 9: p.37–46.
- PU, R., AND S. LANDRY, 2012. A comparative analysis of high spatial resolution IKONOS and WorldView-2 imagery for mapping urban tree species. *Remote Sens. Environ.* 124: p.516–533.
- ROBINSON, D.J., N.J. REDDING, AND D.J. CRISP, 2002. Implementation of a Fast Algorithm for Segmenting SAR Imagery. p.1–48.
- ROERDINK, J., AND A MEIJSTER, 2000. The Watershed Transform: Definitions, Algorithms and Parallelization Strategies. *Fundam. Informaticae* 41: p.187–228.
- THOMAS, E.D., 1995. The cliffs of Kalaupapa. *Wilderness Environ. Med.* 6: p.346–347.
- UPADHYAY, P., S.K. GHOSH, AND A. KUMAR, 2013. High Resolution Temporal Normalized Difference Vegetation. ISPRS Hann. Work. 2013 XL: p.21–24.
- XIAOYING, J., 2012. Segmentation-based image processing system. p.21.

Table 6. Bran-Blanquet Cover Abundance Scores. Primary canopy cover estimates for sample sites

Sam	AA	AM	CE	DI	ES	FM	IS	LC	LO	MA	MM	PG	PL	PO	SC	SE	SJ	SS	ST	OT	Pri	mar	Cov
1	4	.	.	.	3	.	.	SC	
4	5	.	.	ST	
6	5	.	.	ST	
7	1	4	.	.	ST	
9	4	SC	
1	
2	5	.	.	ST	
1	
5	.	1	3	SC	
1	
6	2	.	.	.	1	.	.	2	1	.	.	2	.	.	=	
1	
9	5	.	.	ST	
2	
0	1	5	.	.	1	1	1	.	.	1	.	LC	
2	
6	4	2	ES	
2	
7	1	3	1	.	.	.	1	.	.	AM	
2	
8	4	SC	
2	
9	4	.	.	.	2	.	.	SC	
3	
0	3	.	.	.	4	.	.	ST	
3	
1	3	SC	
3	
2	3	SC	
3	
3	3	.	.	.	3	.	.	=	
3	
4	3	.	.	2	PC	
3	
5	3	.	.	.	2	.	.	SC	
3	
6	1	SC	
3	
8	2	.	1	1	.	1	.	4	.	.	ST	
4	
0	5	SC	
4	.	.	.	2	.	.	1	1	1	1	1	1	.	1	.	.	DI	
4	
2	.	.	5	CE	
4	
3	.	.	5	CE	
4	
4	2	1	.	.	.	4	.	.	ST	
4	
5	2	.	2	.	.	.	3	.	.	ST	
4	
6	4	1	ES	

TABLE 8. SVM model vectors and associated attributes.

	SM	SS D	SMN	SM X	TX R	TXM	TX V	TXE	Attributes
MSB1	8
MSB2	7
MSB3	7
MSB4	7
MSB5	7
MSB6	4
MSB7	4
MSB8	5
TLS1	4
TLS2	6
TLS3	7
TLS4	5
NDVI1	4
HUE	3
SAT	4
INT	7
Bands Computed	15	8	15	10	9	13	8	11	

Abbreviated Key

- | | | |
|--|--------------------------------------|------------------------------|
| MSB1: Multispectral Band 1 – Coastal (400 - 450 nm) | TLS1: Elevation | SM: Spectral Mean |
| MSB2: Multispectral Band 2 – Blue (450 - 510 nm) | TLS2: Per-Cell-Density | SSD: Spectral Std. Deviation |
| MSB3: Multispectral Band 3 – Green (510 - 580 nm) | TLS3: Normalized Canopy Height Model | SMN: Spectral Minimum |
| MSB4: Multispectral Band 4 – Yellow (585 - 625 nm) | TLS4: Reflectance (1,550 nm) | SMX: Spectral Maximum |
| MSB5: Multispectral Band 5 – Red (630 - 690 nm) | NDVI1: NDVI (MSB7 – MSB5) | TXR: Textural Range |
| MSB6: Multispectral Band 6 – Red Edge (705 - 745 nm) | HUE: HUE (RGB color space) | TXM: Textural Mean |
| MSB7: Multispectral Band 7 – Near IR 1 (770 - 895 nm) | SAT: Saturation (RGB color space) | TXV: Textural Variance |
| MSB8: Multispectral Band 8 – Near IR 2 (860 - 1040 nm) | INT: Intensity (RGB color space) | TXE: Textural Entropy |

MS bands derived from Worldview-2 Satellite Platform, TLS bands derived from Reigl VZ-1000 Laser Scanner, HSI and NDVI bands derived from ENVI 5.2

TABLE 9. Classification confidence and estimated coverage area. Confidence values are representative of the predicted confidence for each ROI across all segmented regions for the entire crater.

Class Type	Range (%)	Mean (%)	Std. Dev. (%)	Area (km ²)	Cover Contribution (%)
<i>Erythrina sandwicensi</i>	0.82	0.59	0.22	0.14	5.69
<i>Lantana camara</i> *	0.81	0.54	0.18	0.08	3.32
<i>Schinus terebinthifolius</i>	0.82	0.69	0.22	0.51	20.22
<i>Syzygium cumini</i>	0.83	0.75	0.21	0.82	32.87
Soil Type 1	0.83	0.72	0.26	0.18	7.09
Soil Type 2	0.84	0.62	0.24	0.23	9.14
Soil Type 3	0.81	0.71	0.26	0.09	3.48
Shadow	0.83	0.74	0.21	0.46	18.19

* Indicates native species

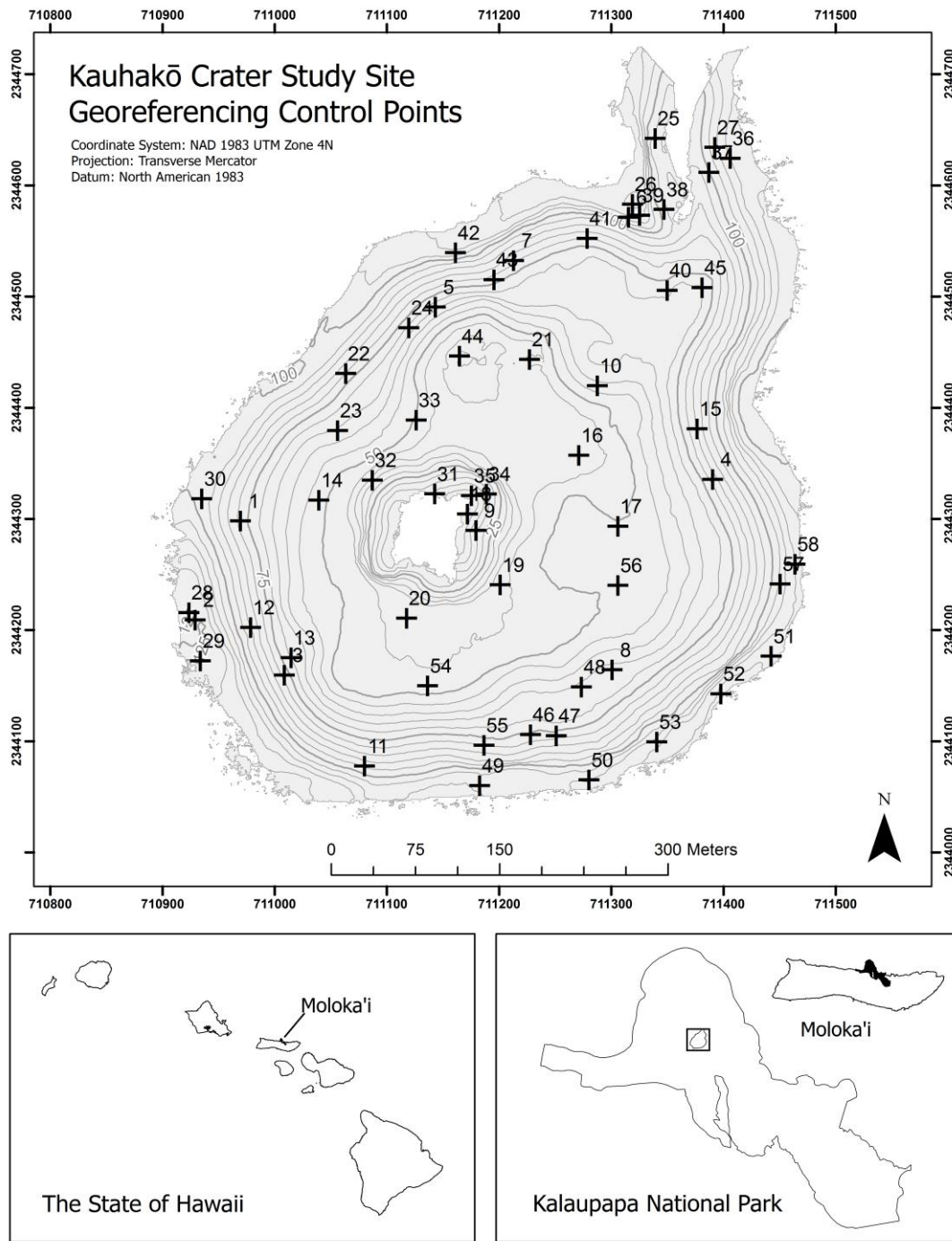


FIGURE 10: Study site showing georeference points used to co-register MS and TLS datasets. TLS derived DTM shown with 5 m contour lines.

Reference Data Collection Sites

Vegetation Height Regime Height Range (m)

	Mostly Bare Earth	0 - 0.6
	Low Shrubs	0.6 - 1.7
	Tall Shrubs	1.7 - 3.6
	Small Trees	3.6 - 6.9
	Medium Trees	6.9 - 12.9
	Tall Trees	12.9 - 23.6
	Sample Point	

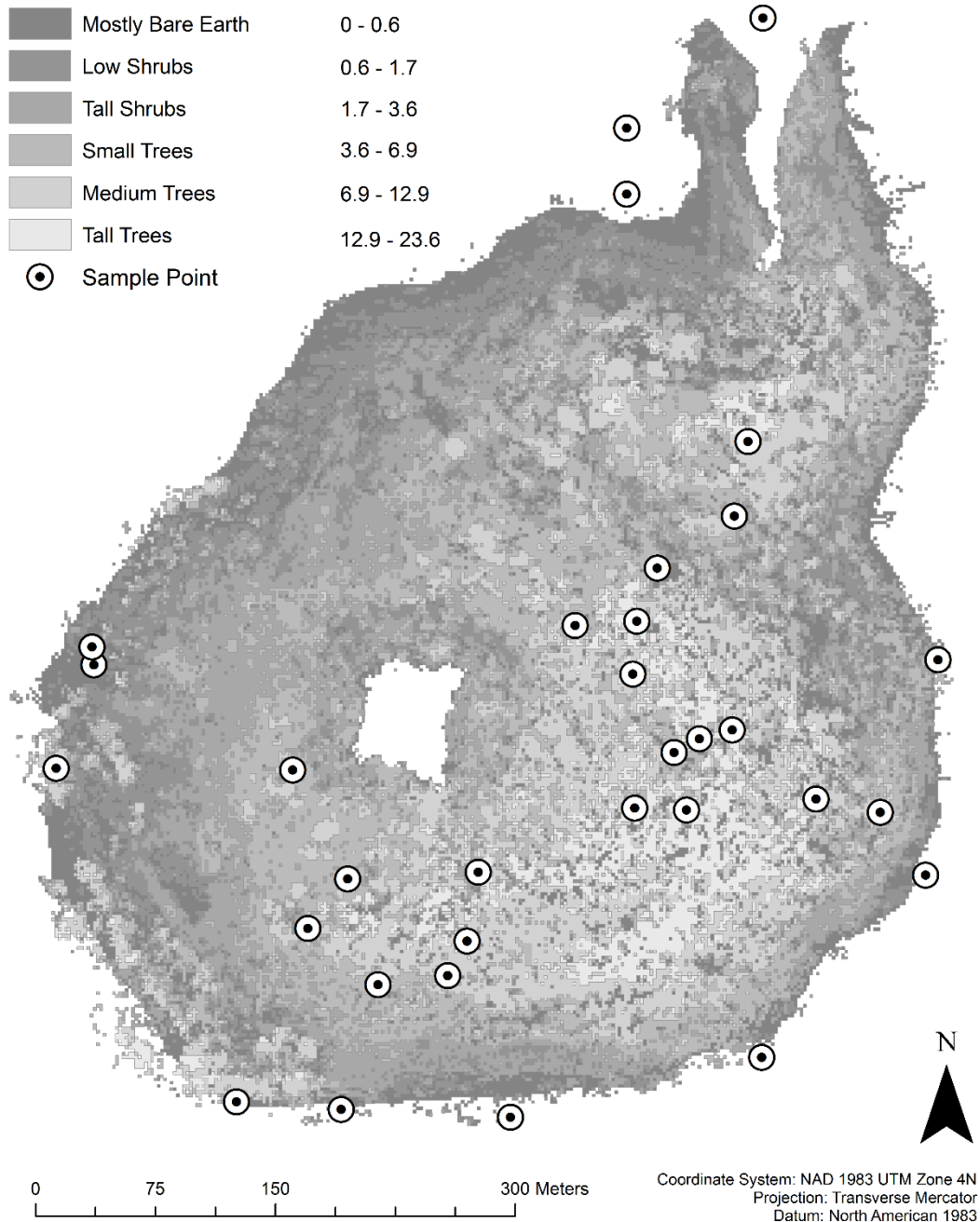


FIGURE 11: Reference data sampling locations. Six randomly generate sample locations per height regime. The northwest quadrat has few sampling points due to low field sampling accessibility. Points outside of the known height regimes were used strictly for validation of classification results.

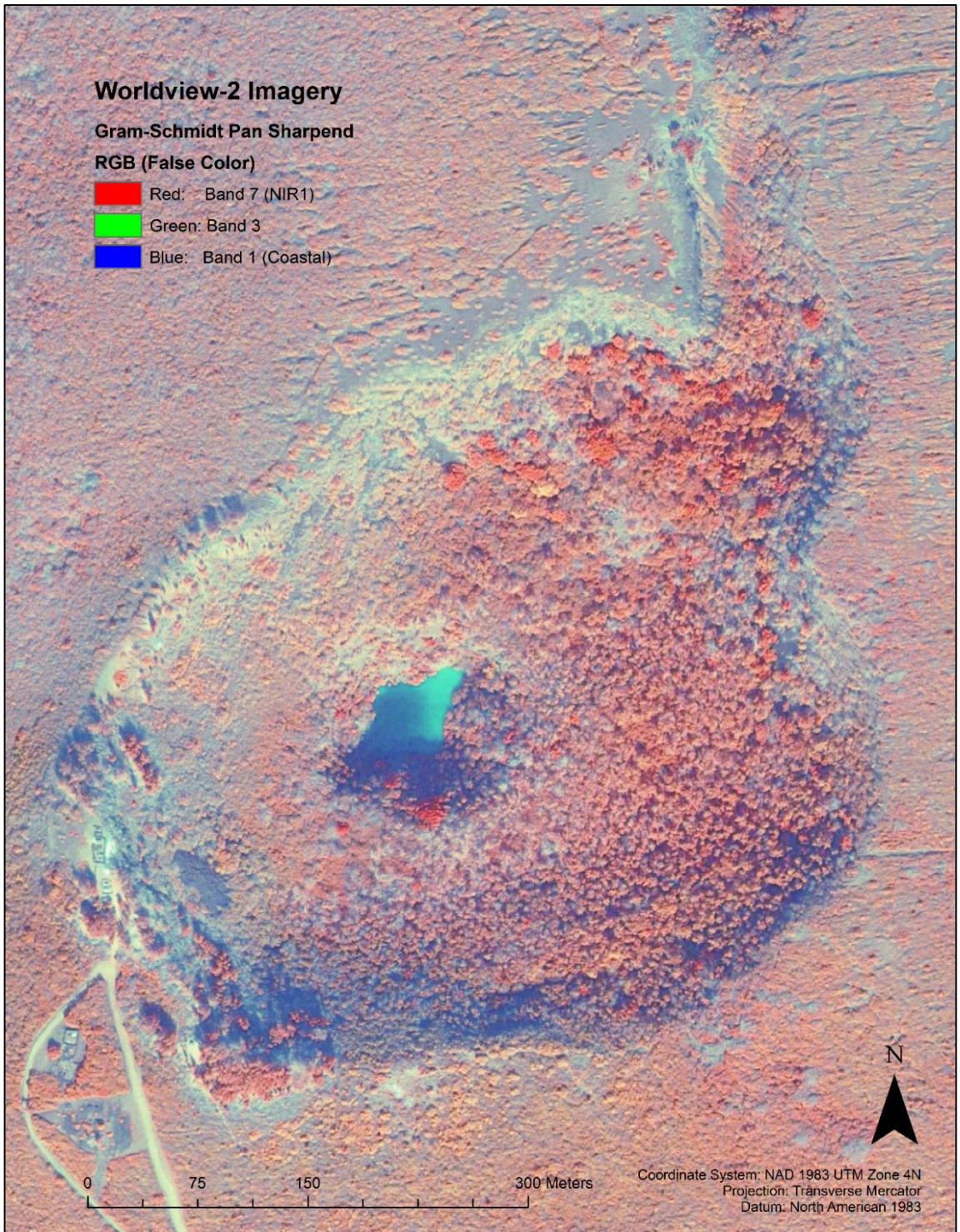


FIGURE 12: *Multispectral Worldview-2 Satellite Imagery. False color image shown using bands (731). Healthy photosynthetic vegetation is contrasted in red against non-vegetation surfaces.*

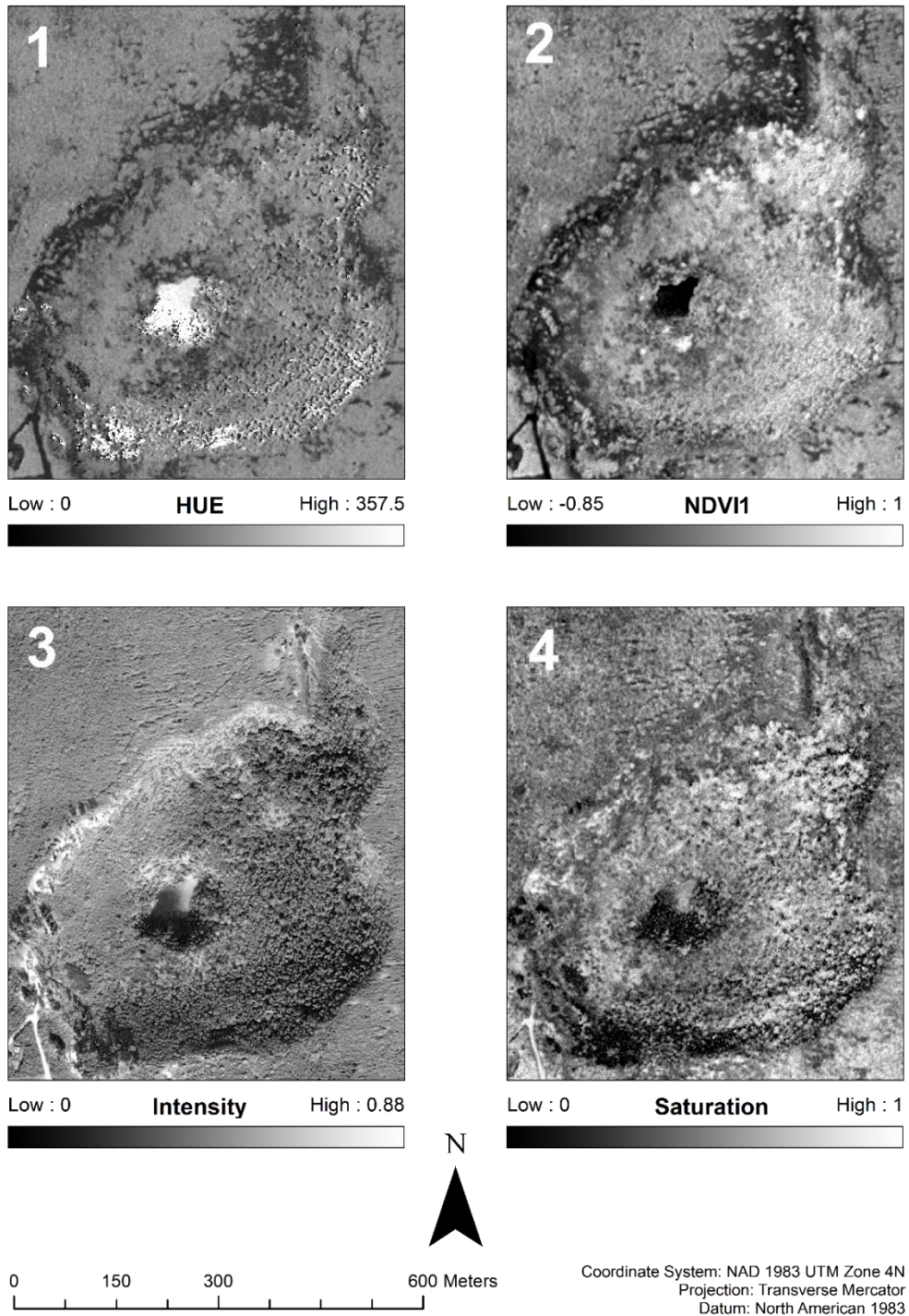


FIGURE 13: *HSI/NDVII Band Values. HUE values ranging from 0 – 360 (1). NDVII Values range from -1 – 1. MSB5 and MSB7 were used to generate this image (2). Intensity values range from 0 – 1 (3). Saturation values range from 0 – 1 (4).*

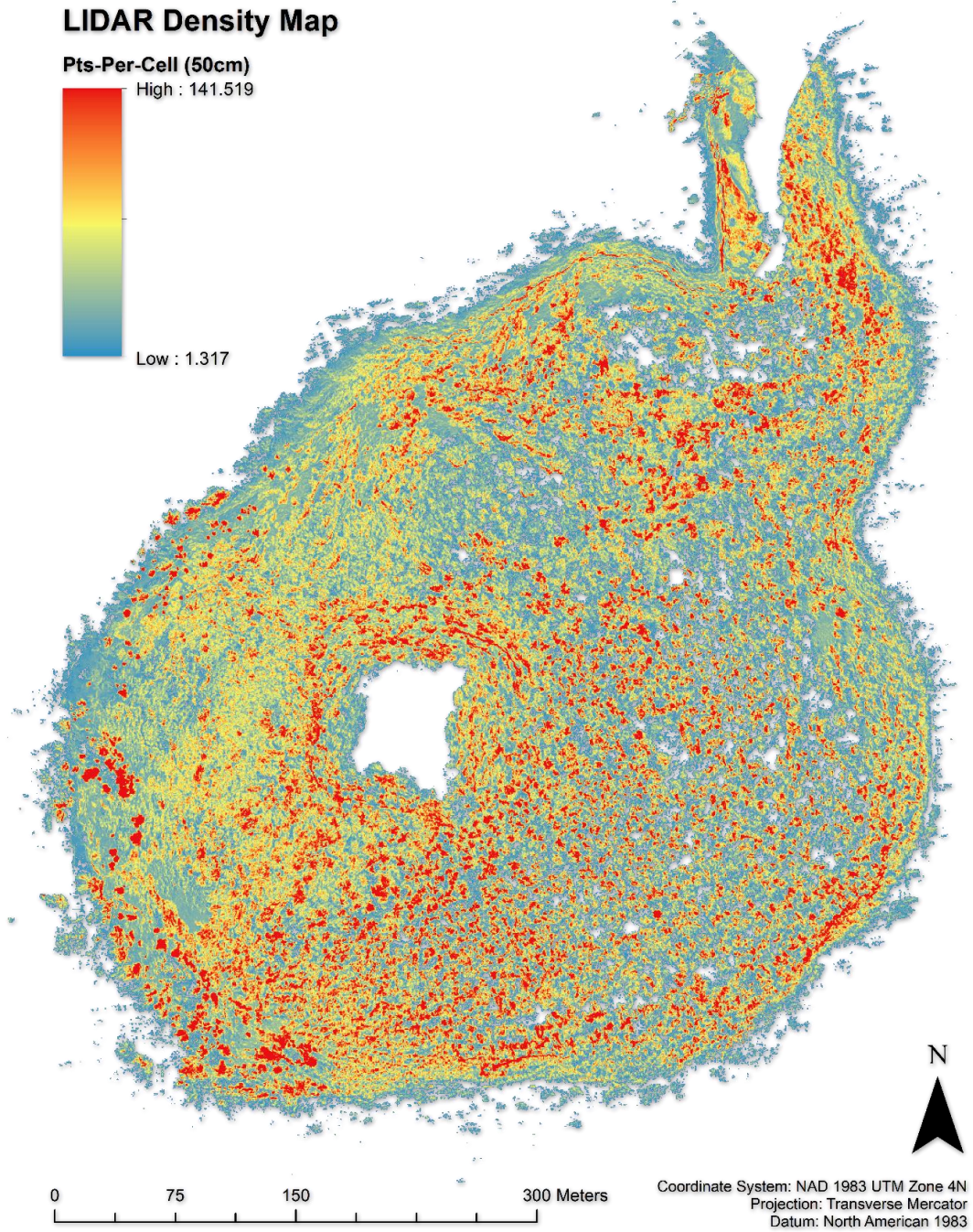


FIGURE 14: (TLS2) Vertical concentration of LiDAR points per raster cell. Areas of high density are indicative of vertical faces including cliffs and tree trunks.

LIDAR Normalized Canopy Height Model (nCHM) Map

Vegetation Height (m)

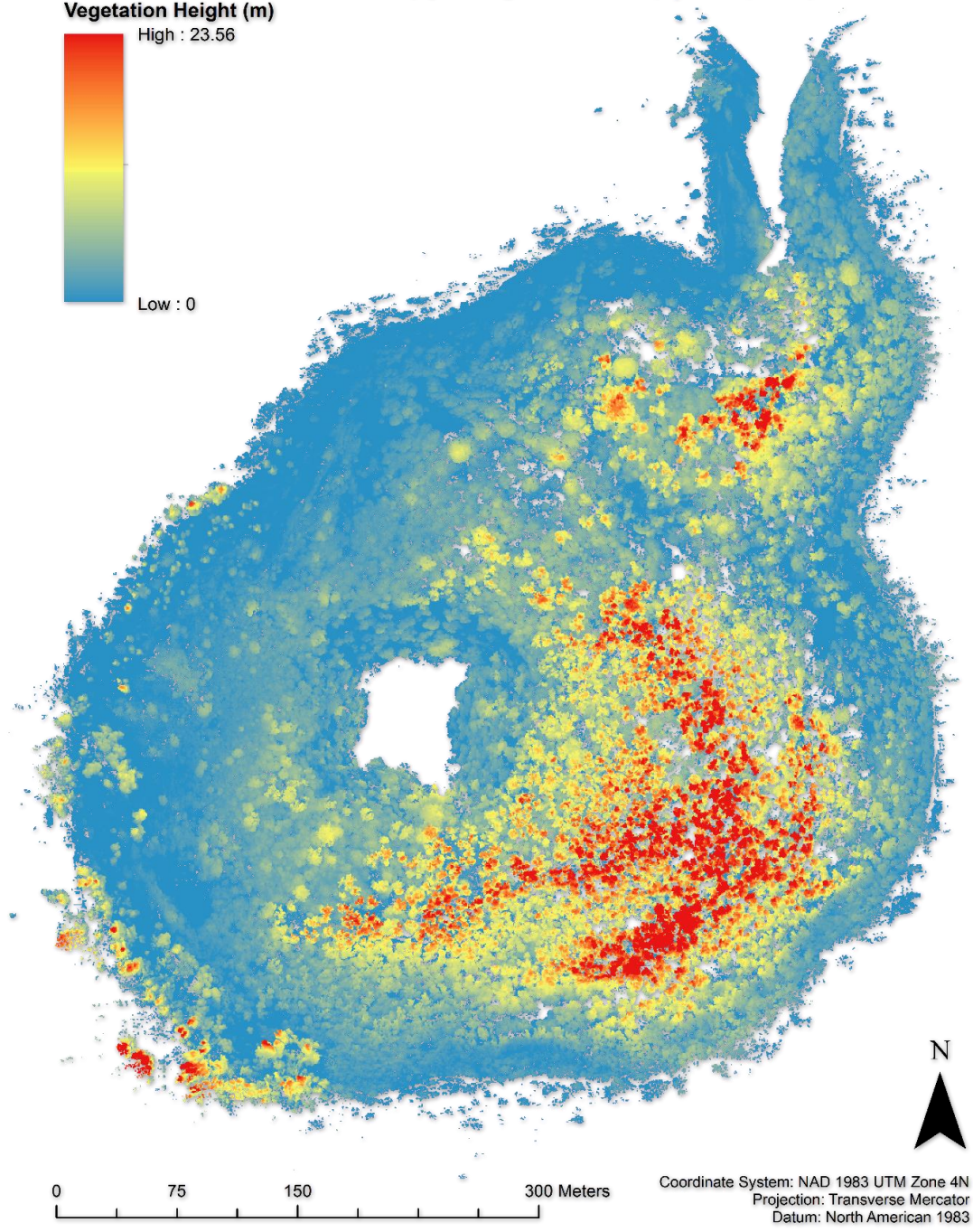
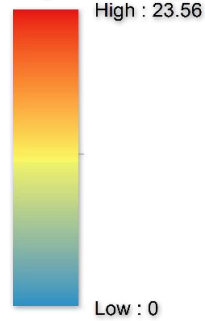


FIGURE 15: (TLS3) Normalized Canopy Height Model. TLS derived vegetation height estimates of the forest canopy surface.

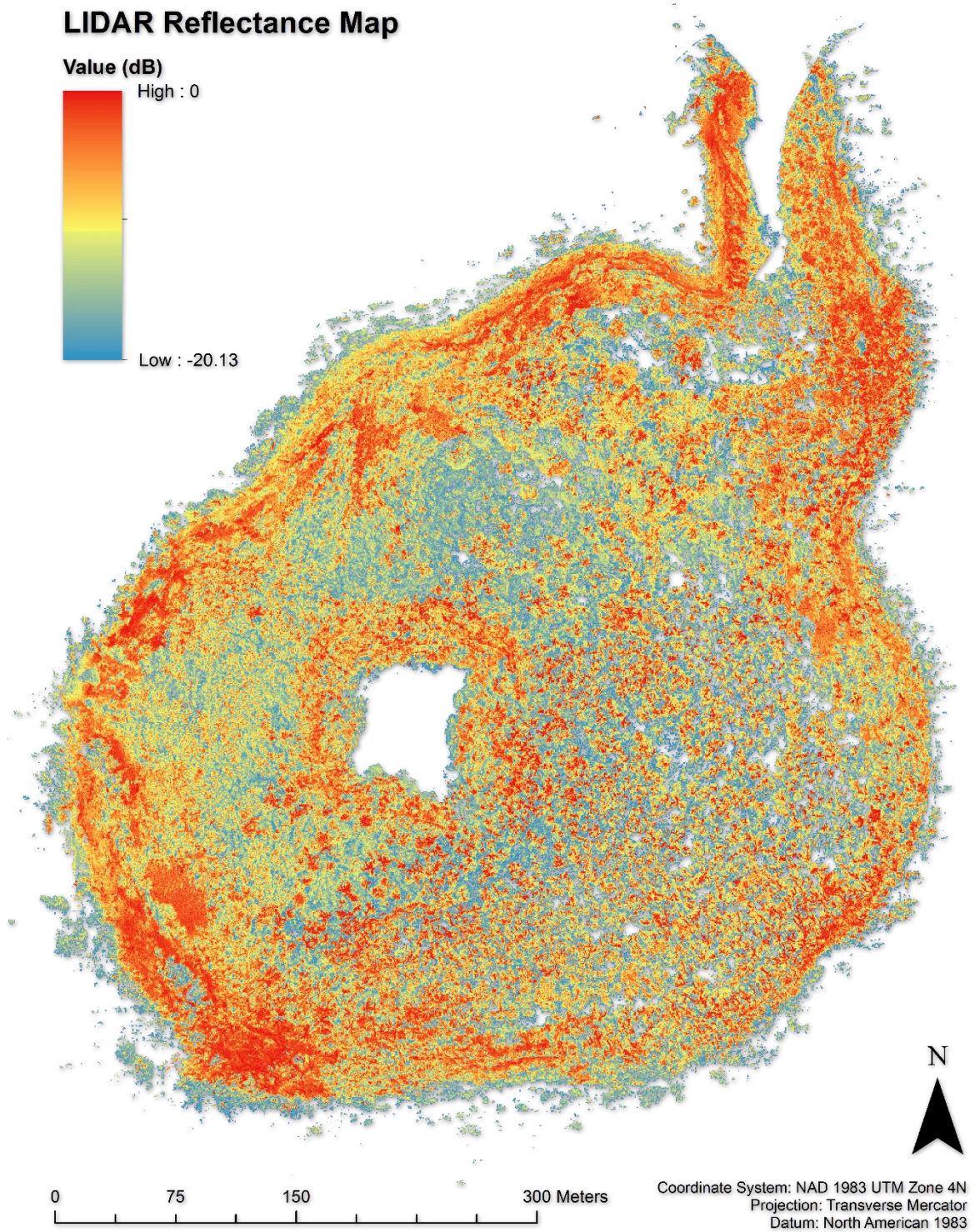


FIGURE 16: (TLS4) Surface reflectance. Bare earth has a significantly greater reflective response compared to vegetation. Green vegetation reflectance is moderate to low. These difference enhance class distinctions.

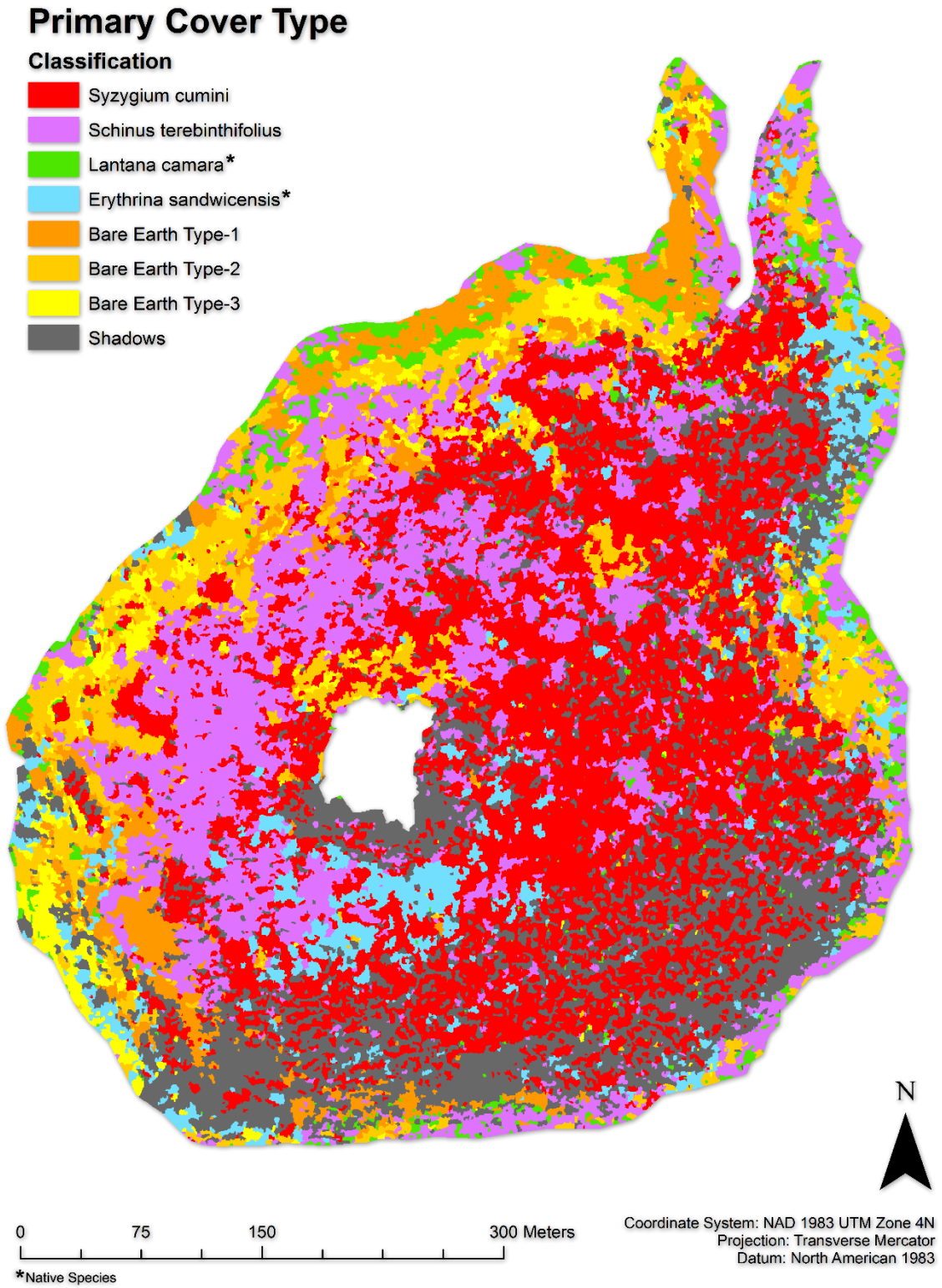


FIGURE 17: Primary canopy cover type classification results. More than 85% of the vegetative community is composed of non-native species while roughly 15% is composed of native species (TABLE 4).

CHAPTER 4. CONCLUSION

TLS was used to develop high resolution surface models of both occluded terrain and forested canopy cover in a culturally restricted volcanic crater on the Island of Molokai in Hawaii. Characterization of these surfaces was incorporated into a vegetation study using remotely sensed satellite imagery to describe and identify forest components within the crater in an effort to establish a set of baseline conditions for long term monitoring. The resulting datasets demonstrate the effective use of a data fusion approach to derive enhanced classification results in a small region of interest which would be typically susceptible to physical, spatial and spectral sampling deficiencies.

In Chapter 2, we used TLS to scan and document the unbiased structure of a densely vegetated forest community. Due to the high degree of canopy closure, photogrammetrically derived DEMs are non-existent as well as GPS surveys in light of cultural access restrictions. We used high density TLS to exhaustively scan the crater structure from six locations outside the restricted boundary. We then used a combination of spatial filtering techniques to extract ground points which were then used to build an interpolated surface of the terrain with a 50 cm spatial resolution. Next we used the DTM to derive an nCHM of the vegetative canopy to assess the vegetative height regimes of the forest community.

The relative success of our scanning approach, filtering techniques and terrain building workflow exemplify the use of TLS as a viable approach to surface modeling in regions with access restrictions where conventional survey techniques are rendered impractical. While photogrammetric models are capable of resolving coarse to moderate resolution 3D characteristics of canopy surfaces, without knowledge of the underlying

terrain it is impossible to make assumptions regarding vegetation heights and any affiliated statistics pertaining to delineating measures of age, growth, and distribution. Furthermore, the success of the outlined modeling approaches is performed using open source software solutions that are freely available and open to further development, possibly paving the way for robust techniques built on the same foundational approaches.

The resulting DTM is not without its imperfections. Although we used a slow scanning speed and six scan locations to produce a high density point cloud with an average point spacing of 10 cm, there was still evidence of artifacts caused by occlusion. We speculate that the occlusion of these regions could have likely been avoided had we added more scan positions to increase the likelihood of receiving ground returns in those regions. However, intuition tells us that this may have likely resulted in a systemic error coefficient without the use of precision targets to reduce our alignment errors. Had we used precision targets, they would have had to be very large to produce an adequate amount of registered points.

In Chapter 3, we integrate LiDAR datasets developed in chapter 2 with remotely sensed multispectral satellite imagery. The integration of high resolution structural information with high spectral resolution imagery enabled us to produce a representative classification map of the forest structure not easily achievable using each dataset exclusively. First we segmented the MS imagery using edge delineating algorithms based purely on mean spectral values from the three most separable MS imagery bands and three synthetic bands (HSI) generated from the entire (8-band) MS dataset. Smaller regions are merged together using a similarity threshold to aggregate small regions and reduce the overall segmentation count. A usable subset of our reference data was used to

identify regions of interest that were representative of the determined forest types. These ROIs were then used to extract endmember classifiers from the input datasets. We then processed all datasets using an SVM model to identify and match the vegetation profiles throughout the crater to that of our training regions.

While the spectral resolution of our imagery provided adequate contrast to detect feature boundaries, we found it necessary to integrate structural TLS datasets that described elevation, canopy height, density and reflectivity to identify distinguishing differences between forest stands. Without the addition of these datasets, there was a high degree of misclassification due in part to the spectral and textural homogeneity associated with our ROIs. Confidence estimates for predicted canopy cover types revealed a stratified dominance throughout the crater by non-native vegetation.

Within the applied scope of this research, we believe qualitative improvements in both TLS and MS imagery dataset could lead to higher prediction confidence and possibly the extension of our data fusion methods to sub-canopy regions. Our methods could clearly benefit from two areas of improvement. The first being the addition of subsequent scan locations from above and below the canopy to improve estimates of vegetation height, DTM surface, and reduce occlusion effects. The second being the use of imagery with a higher bit-depth to improve the distinction between partial pixel class memberships. Lastly, minimization of the temporal offset between TLS scanning and MS imagery capture times could reduce misclassifications errors stemming from ecological change.

This research can be immediately built upon to develop more efficient algorithms for extracting ground surfaces from dense point cloud data in highly vegetated regions.

While many approaches to vegetation analysis focus on the use of aerial LiDAR for integration with MS imagery, TLS has yet to receive the same level of attention. As a form of remote sensing, TLS is an extremely versatile tool which can produce exceedingly dense datasets over relatively smaller regions. The convergence of active and passive remote sensing platforms is closely approaching as improvements in sensing capabilities continue to expand. Data fusion may in fact one day be the common method of analysis in fields of remote sensing, thus the exploration the practical applications for estimates of ecosystem services and earth processes will most likely benefit greatly from continued research in similar fields study.

LITERATURE CITED

- BARNHART, T., AND B. CROSBY, 2013. Comparing Two Methods of Surface Change Detection on an Evolving Thermokarst Using High-Temporal-Frequency Terrestrial Laser Scanning, Selawik River, Alaska. *Remote Sens.* 5: p.2813–2837.
- BOYD, D.S., AND G.M. FOODY, 2011. An overview of recent remote sensing and GIS based research in ecological informatics. *Ecol. Inform.* 6: p.25–36.
- BUCHROITHNER, M.F., AND T. GAISECKER, 2009. Terrestrial Laser Scanning for the Visualization of a Complex Dome in an Extreme Alpine Cave System. *Photogramm. - Fernerkundung - Geoinf.* 2009: p.329–339.
- CHEN, L., T. CHIANG, AND T. TEO, 2005. Fusion of LIDAR data and high resolution images for forest canopy modelling. *In* 26th Asian Conference on Remote Sensing and 2nd Asian Space Conference. p. 7, Ha Noi, Vietnam.
- CLARK, D.B., J.M. READ, M.L. CLARK, A.M. CRUZ, M.F. DOTTI, AND D.A. CLARK, 2004. Application of 1-m and 4-m resolution satellite data to ecological studies of tropical rain forests. *Ecol. Appl.* 14: p.61–74.
- COSTANTINO, D., AND M.G. ANGELINI, 2013. Production of DTM quality by TLS data. *Eur. J. Remote Sens.* 46: p.23.
- DELPARTE, D.M., M. BELT, C. NISHIOKA, N. TURNER, R.T. RICHARDSON, AND T. ERICKSEN, 2014. Monitoring tropical alpine lake levels in a culturally sensitive environment utilizing 3D technological approaches. *Arctic, Antarct. Alp. Res.* 46: p.709–718.
- GLENN, N.F., L.P. SPAETE, T.T. SANKEY, D.R. DERRYBERRY, S.P. HARDEGREE, AND J.J. MITCHELL, 2011. Errors in LiDAR-derived shrub height and crown area on sloped terrain. *J. Arid Environ.* 75: p.377–382.
- GOULD, W., 2000. Remote Sensing of Vegetation, Plant Species Richness, and Regional Biodiversity Hotspots. *Ecol. Appl.* 10: p.1861–1870.
- GREENE, L.W., 1985. Exile in paradise: The isolation of Hawai'i's leprosy victims and development of Kalaupapa settlement, 1865 to present. [Denver] Branch Planning, Alaska/Pacific Northwest/Western Team, U.S. Dept. Inter. Natl. Park Serv. Denver Serv. Cent.p.728.
- GUARNIERI, A., A. VETTORE, F. PIROTTI, AND M. MARANI, 2009. Filtering of TLS Point Clouds for the Generation of DTM in Salt-Marsh Areas. XXXVIII: p.293–298.

- JONES, T.G., N.C. COOPS, AND T. SHARMA, 2010. Assessing the utility of airborne hyperspectral and LiDAR data for species distribution mapping in the coastal Pacific Northwest, Canada. *Remote Sens. Environ.* 114: p.2841–2852.
- KASPERSKI, J., C. DELACOURT, P. ALLEMAND, P. POTERAT, M. JAUD, AND E. VARREL, 2010. Application of a Terrestrial Laser Scanner (TLS) to the study of the S??chilienne landslide (Is??re, France). *Remote Sens.* 2: p.2785–2802.
- KIM, S., 2007. *Individual tree species identification using LIDAR-derived crown structures and intensity data*. University of Washington.
- KIRCH, P. V, 2002. From the “cliffs of Keolewa”to the “sea of Papaloa”: an archaeological reconnaissance of portions of the Kalaupapa National Historical Park, Moloka‘i, Hawaiian Islands. *Ocean. Archaeol. Lab. Spec. Publ.*
- KIRCH, P. V, 2007. Hawaii as a model system for human ecodynamics. *Am. Anthropol.* 109: p.8–26.
- KURASHIMA, N., AND P. V KIRCH, 2011. Geospatial modeling of pre-contact Hawaiian production systems on Moloka‘i Island, Hawaiian Islands. *J. Archaeol. Sci.* 38: p.3662–3674.
- LATIF, Z.A., I. ZAMRI, AND H. OMAR, 2012. Determination of tree species using Worldview-2 data. *In Signal Processing and its Applications (CSPA), 2012 IEEE 8th International Colloquium on.* pp. 383–387.
- LEEUWEN, M., AND M. NIEUWENHUIS, 2010. Retrieval of forest structural parameters using LiDAR remote sensing. *Eur. J. For. Res.* 129: p.749–770.
- MCCOY, M.D., 2005. The development of the Kalaupapa field system, Moloka‘i Island, Hawai‘i. *J. Polyn. Soc.* 114: p.339–358.
- MORALES, R.M., 2012. *Using Remotely Sensed Imagery for Forest Resource Assessment and Inventory* J. A. Blanco (Ed.), InTech.
- NICHOL, J., AND L. HANG, 2008. The influence of DEM accuracy on topographic correction of Ikonos satellite images. *Photogramm. Eng. Remote*
- PAPASAIKA, H., AND E. BALTSAVIAS, 2009. Fusion of LiDAR and Photogrammetric Generated Digital Elevation Models. *In Proc. ISPRS Hannover Workshop on High-Resolution Earth Imaging for Geospatial Information, Hannover, Germany.* pp. 2–5, Citeseer.
- PRICE, B.J.P., J.D. JACOBI, S.M. GON, D. MATSUWAKI, L. MEHRHOFF, W. WAGNER, M. LUCAS, B. ROWE, AND U.S.G. SURVEY, 2012. Mapping Plant Species Ranges in the Hawaiian Islands — Developing a Methodology and Associated GIS Layers.

- PU, R., AND S. LANDRY, 2012. A comparative analysis of high spatial resolution IKONOS and WorldView-2 imagery for mapping urban tree species. *Remote Sens. Environ.* 124: p.516–533.
- SAKAI, A.K., W.L. WAGNER, AND L.A. MEHRHOFF, 2002. Patterns of endangerment in the Hawaiian flora. *Syst. Biol.* 51: p.276–302.
- SCHENK, T., AND B. CSATHÓ, 2002. Fusion of LIDAR data and aerial imagery for a more complete surface description. *Int. Arch. Photogramm. Remote Sens. Spat. Inf. Sci.* 34: p.310–317.
- SINGH, K.K., J.B. VOGLER, D.A. SHOEMAKER, AND R.K. MEENTEMEYER, 2012. LiDAR-Landsat data fusion for large-area assessment of urban land cover: Balancing spatial resolution, data volume and mapping accuracy. *ISPRS J. Photogramm. Remote Sens.* 74: p.110–121.
- STOCK, G.M., N. LUCO, B.D. COLLINS, E.L. HARP, P. REICHENBACH, K.L. FRANKEL, N.P. SERVICE, Y.N. PARK, E. PORTAL, U.S.G. SURVEY, AND M. PARK, 2012. Quantitative rock-fall hazard and risk assessment for Yosemite Valley , Yosemite National Park , California. USGS - Yosemite Natl. Park - PhD 30332: .
- ST-ONGE, B., C. VEGA, R.A. FOURNIER, AND Y. HU, 2008. Mapping canopy height using a combination of digital stereo-photogrammetry and lidar. *Int. J. Remote Sens.* 29: p.3343–3364.
- SYED, S., P. DARE, AND S. JONES, 2005. Automatic classification of land cover features with high resolution imagery and lidar data: an object-oriented approach. *In ... : the national biennial Conference of the ...* pp. 512–522, Melbourne: Melbourne: Spatial Science Institute.
- THOMAS, E.D., 1995. The cliffs of Kalaupapa. *Wilderness Environ. Med.* 6: p.346–347.
- VARGA, T.A., AND G.P. ASNER, 2008. Hyperspectral and LiDAR remote sensing of fire fuels in Hawaii Volcanoes National Park. *Ecol. Appl.* 18: p.613–623.
- WULDER, M.A., R.J. HALL, N.C. COOPS, AND S.E. FRANKLIN, 2004. High Spatial Resolution Remotely Sensed Data for Ecosystem Characterization. *Bioscience* 54: p.511–521.